



MARMARA UNIVERSITY
FACULTY OF ENGINEERING



Comparison of Sound Insulation Performance of Water Drop and Trapezoidal Sound Barriers

Arif DOĞAN

GRADUATION PROJECT REPORT
Department of Mechanical Engineering

Supervisor
Prof. Dr. Paşa YAYLA

ISTANBUL, 2024



MARMARA UNIVERSITY
FACULTY OF ENGINEERING



**Comparison of Sound Insulation Performance of Water Drop and
Trapezoidal Sound Barriers**
by

Arif DOĞAN

June 26, 2024, İstanbul

**SUBMITTED TO THE DEPARTMENT OF MECHANICAL ENGINEERING IN
PARTIAL FULFILLMENT OF THE REQUIREMENTS FOR THE DEGREE**

OF

BACHELOR OF SCIENCE

AT

MARMARA UNIVERSITY

The author(s) hereby grant(s) to Marmara University permission to reproduce and to distribute publicly paper and electronic copies of this document in whole or in part and declare that the prepared document does not in anyway include copying of previous work on the subject or the use of ideas, concepts, words, or structures regarding the subject without appropriate acknowledgement of the source material.

Signature of Author(s)..... **Arif DOĞAN**.....

Department of Mechanical Engineering

Certified by..... **Prof.Dr. Paşa YAYLA**.....

Project Supervisor, Department of Mechanical Engineering

Accepted by..... **Prof.Dr. Bülent EKİCİ**.....

Head of the Department of Mechanical Engineering

ACKNOWLEDGEMENT

I extend my deepest gratitude to my mentor, Prof. Dr. Paşa YAYLA, whose insightful guidance and unwavering support, both academically and personally, have been instrumental in the development of this thesis.

I extend my heartfelt gratitude to Ahmet ASLANDAĞ and Samet KOCA for their invaluable assistance throughout the completion of this thesis project. Their support, on behalf of Kasso Mühendislik San. ve Tic. A.Ş., proved instrumental in navigating the challenges and achieving the objectives of this endeavour. Also, I would like to express my gratitude to Kasso Mühendislik San. ve Tic. A.Ş. for providing us with the project's concept and relevant documents. Their collaboration and assistance have been invaluable to us.

With sincere appreciation, I would like to extend my gratitude to Armin HASHEMI for his invaluable assistance during the analysis process and for his guidance in learning COMSOL. His expertise and support were integral to the successful completion of this project.

June, 2024

Arif DOĞAN

CONTENTS

| | |
|---|------|
| ACKNOWLEDGEMENT..... | iii |
| CONTENTS | iv |
| ABSTRACT | iv |
| SYMBOLS | v |
| ABBREVIATIONS | vi |
| LIST OF FIGURES | vii |
| LIST OF TABLES | viii |
| 1. INTRODUCTION AND PROBLEM BACKGROUND | 1 |
| 1.1. INTRODUCTION | 1 |
| 1.2. BACKGROUND | 1 |
| 1.2.1. Problem Statement..... | 2 |
| 1.2.2. Literature Review | 2 |
| 1.2.3. Material of Sound Barriers: | 5 |
| 1.2.4. Trapezoidal Sound Barriers: Design, Performance, and Applications: | 8 |
| 1.2.5. Droplet Model for Sound Barriers: Aesthetic and Acoustic Advancements: | 9 |
| 2. ANALYSIS CALCULATIONS BACKGROUND | 10 |
| 2.1. ACOUSTIC-STRUCTURE ANALYSIS..... | 10 |
| 2.2. Sound Transmission Loss Analysis | 12 |
| 3. ANALYSIS METHOD, SETUP AND RESULTS | 18 |
| 3.1. EXPERIMENTAL ANALYSIS SETUP..... | 18 |
| 3.1.1. Global Definitions | 18 |
| 3.1.2. Selection | 21 |
| 3.1.3. Materials and domain | 22 |
| 3.1.4. Pressure Acoustics, Frequency Domain | 25 |
| 3.1.5. Multiphysics | 26 |
| 3.1.6. Mesh 1 | 27 |
| 3.1.7. Study 1 | 27 |
| 3.1.8. Results | 28 |
| 3.1.9. Datasets | 29 |

| | |
|---|----|
| 3.1.10. Plot Groups for droplet..... | 30 |
| 3.1.11. Plot Groups for trapez | 33 |
| 4. RESULTS AND COMPARING | 36 |
| 4.1. LIMITATIONS AND CONSIDERATIONS | 37 |
| 4.2. OVERALL COMPARISON | 38 |
| 4.3. EVALUATION OF CURRENT WORK FROM MUDEK PERSPECTIVE..... | 38 |
| 4.3.1. Economic Analysis | 38 |
| 4.3.2. Real-Life Conditions | 39 |
| 4.3.3. Producibility | 39 |
| 4.3.4. Constraints..... | 39 |
| 5. CONCULUSION | 41 |
| REFERENCES AND AUXILARY RESOURCES..... | 42 |
| APPENDICES..... | 45 |

ABSTRACT

The project is an R&D initiative conducted in collaboration with Marmara University and Kasso Mühendislik San. ve Tic. A.Ş., focusing on the development of innovative noise barriers for outdoor environments. Specifically, the project will explore the freeform design of sheet metal-based noise barriers, analysing both their static and acoustic properties. The research will be particularly centered on evaluating the effectiveness of these barriers in mitigating noise pollution in motorway and railway environments.

Keywords: Metallic noise barriers, Freeform surface design, Static and acoustic analysis, Outdoor sound insulation

SYMBOLS

| | |
|-----------|---|
| D_e | insertion loss: $[D_e] = \text{dB}$ |
| D_z | barrier attenuation: $[Dz] = \text{dB}$ |
| L_p | sound pressure level: $[Lp] = \text{dB}$ |
| Z | wall impedance: $[Z] = \text{mN s}^{-3}$ |
| α | absorption coefficient: $[\alpha] = \text{dimensionless parameter with } 0 \leq \alpha \leq 1$ |
| c | speed of sound in the fluid: $[c] = \text{ms}^{-1}$ |
| δ | path-length difference: $[\delta] = \text{m}$ |
| f | frequency: $[f] = \text{Hz}$ |
| λ | wavelength: $[\lambda] = \text{m}$ |
| p | pressure: $[p] = \text{Pa}$ |
| ρ_0 | equilibrium density of the fluid: $[\rho_0] = \text{kg/m}^3$ |
| Ω | omega, angular frequency $[\omega] = \text{rad}\cdot\text{s}^{-1}$ |
| Pa | Pascal |

ABBREVIATIONS

BEM - Boundary Element Method

FEM - Finite Element Method

PML - Perfectly Matched Layer

STL - Sound Transmission Loss

I_x_room - Sound intensity, positive x direction

P_in - Incident power on the concrete surface

P_in_proom - Incident power (room pressure)

p_ms_th - Theoretical mean square pressure in source room (limit N->infinity)

P_in_th - Theoretical incident power (limit N->infinity)

P_tr - Transmitted power0

ASTM - American Society for Testing and Materials.

ISO - Abbreviation for International Organization for Standardization.

T₆₀ - Reverberation time

SIL - Sound Intensity Level

EDT - Early Decay Time

SPL - Sound Pressure Level

RMS - Root mean square

LIST OF FIGURES

| | |
|--|----|
| Figure 1.1 Basic representation of noise barrier effect..... | 4 |
| Figure 1.2 Sound level as dB..... | 5 |
| Figure 1.3 Trapez model view of noise barrier..... | 8 |
| Figure 1.4 CAD drawing of trapezoidal noise barrier. | 8 |
| Figure 1.5 Droplet Model view 1 | 9 |
| Figure 1.6 Droplet Model view 2 | 9 |
| Figure 2.1 Frequency dependent sound transmission regions of a panel | 12 |
| Figure 2.2 The two variations of the two-room configuration for measuring the sound transmission loss. Top: source and receiver reverberation rooms. Bottom: source reverberation room and receiver anechoic room..... | 14 |
| Figure 3.1 Front face selection | 21 |
| Figure 3.2 Back face selection..... | 22 |
| Figure 3.3 Perfectly matched layer selection..... | 22 |
| Figure 3.4 Geometry drawing view | 23 |
| Figure 3.5 Air domain selection | 24 |
| Figure 3.6 Aluminum domain selection | 24 |
| Figure 3.7 Pressure Acoustics, Frequency Domain Selection | 25 |
| Figure 3.8 Solid mechanics domain selection | 25 |
| Figure 3.9 Acoustic-Structure Boundary selection..... | 26 |
| Figure 3.10 Mesh views..... | 27 |
| Figure 3.11 Calculation data points and locations view | 28 |
| Figure 3.12 Indicated Power graph..... | 30 |
| Figure 3.13 STL Sound Transmission Loss Graph | 30 |
| Figure 3.14 Acoustic Pressure (acpr)..... | 31 |
| Figure 3.15 Sound Pressure Level (acpr) | 31 |
| Figure 3.16 Acoustic Pressure, Isosurfaces (acpr)..... | 32 |
| Figure 3.17 Stress (solid)..... | 32 |
| Figure 3.18 STL: P_in/P_tr (1/3 octaves)..... | 33 |
| Figure 3.19 Acoustic Pressure (acpr)..... | 33 |
| Figure 3.20 Sound Pressure Level (acpr) | 34 |
| Figure 3.21 Acoustic Pressure, Isosurfaces (acpr)..... | 34 |
| Figure 3.22 Stress (solid)..... | 35 |
| Figure 3.23 Indicated Power (three methods)..... | 35 |
| Figure 4.1Comparison of analysis results of water drop and trapezoidal design with actual experimental results of trapezoidal design. | 37 |

LIST OF TABLES

| | |
|--|----|
| Table 2-1 Acoustics Domain Data..... | 10 |
| Table 2-3 Radiation Boundary Condition Settings..... | 11 |
| Table 3-1 Parameters table | 19 |
| Table 3-2 Variables | 20 |
| Table 3-3 Octave band results | 29 |

1. INTRODUCTION AND PROBLEM BACKGROUND

1.1. INTRODUCTION

Urban areas are increasingly grappling with the issue of noise pollution, which significantly detracts from residents' quality of life. According to a 2020 report from the European Environment Agency, a substantial portion of the population continues to endure high levels of noise exposure (European Environment Agency, 2020, p. 86). Reducing noise pollution can decrease the likelihood of developing indirect illnesses later in life, thus improving our quality of life. One of the primary solutions is to reduce noise at its source, although this may not always be feasible to the desired extent. Therefore, taking individual protective measures is important. Sound barriers have long been effective in mitigating both visual and auditory pollution, providing benefits to individuals in urban areas.

The main objective of the project is to compare the sound insulation performance of two different designs, a trapezoidal and a water drop design, in an analysed environment. The project aims to improve the functionality of existing noise barriers and determine which of these two designs provides more effective sound insulation. Accordingly, the main focal points are: Comparison of Designs, Performance Analysis, and Evaluation of Results.

In order to achieve these goals, the project is carried out as a joint R&D project between Marmara University and Kasso Mühendislik San. ve Tic. A.Ş. as a joint R&D project. The project is focused on analysing the sound insulation performance of two different designs, trapezoidal and water drop-shaped.

The project offers an innovative approach to noise barriers, emphasising a metallic design as opposed to traditional materials such as glass or plastic composites. This transition simplifies manufacturing processes as well as increases durability and resistance to external factors such as weather conditions. Furthermore, the aim of the project is to provide better sound insulation and overall efficiency by identifying the one with better performance in terms of acoustic and static analyses. By emphasising industrial R&D and technological advancement, the project aims to provide a superior alternative compared to existing noise barriers, improving durability, resistance and performance.

1.2. BACKGROUND

The escalating concerns surrounding noise pollution in urbanized areas have underscored the critical role of outdoor noise barriers. Traditional designs, primarily crafted from materials like glass and plastic composites, have proven effective but are not without limitations. In response to these challenges, a collaborative research initiative between Marmara University and Kasso Mühendislik San. ve Tic. A.Ş. has been launched.

As a pivotal decision in the course of this project, a comparative analysis of two distinct designs has been deemed essential. The chosen designs for evaluation are the trapezoidal design and the droplet (waterdrop) design. These designs, characterized by their unique shapes, will undergo thorough scrutiny utilizing the advanced capabilities of the COMSOL Multiphysics software.

This research will not only rely on computational simulations but will also integrate real-world data and experimental test results. The juxtaposition of the trapezoidal and droplet designs will be a central focus, aiming to identify which design offers superior performance in terms of sound insulation, durability, and overall efficiency.

By incorporating both numerical simulations and empirical evidence, the project aspires to provide a comprehensive understanding of the comparative advantages and limitations of the two selected designs. This approach ensures a robust and practical foundation for the subsequent phases of the project, aligning with the overarching goal of advancing noise barrier technology for a more effective and sustainable urban environment.

1.2.1. Problem Statement

In the realm of sound barrier design, the trapezoidal system has been widely adopted for its ease of production and cost-effectiveness. However, we believe that exploring an alternative in the form of the droplet model could yield superior results, both in terms of visual aesthetics and sound insulation. This comparison aims to assess whether the droplet model, deemed more intricate and potentially effective, could provide a compelling alternative to the commonly used trapezoidal system. The investigation considers factors such as ease of production, cost, visual appeal, and acoustic performance to discern the feasibility and advantages of transitioning from the conventional trapezoidal design to the innovative droplet model. This research addresses an existing gap in exploring alternative sound barrier designs, offering a unique opportunity to enhance both functionality and aesthetics in noise control technology.

1.2.2. Literature Review

The literature review is structured into three key subtopics, each delving into various aspects pertinent to sound barriers. This segment offers an in-depth comprehension of the subject matter, presenting a comparative analysis of diverse existing literature within the field of sound barrier design.

1.2.2.1. Sound Barriers and Their Role in Noise/Sound Mitigation:

Sound barriers play a pivotal role in addressing the pervasive issue of noise pollution, offering a practical solution to mitigate the adverse effects of excessive environmental noise. This subtopic aims to provide a comprehensive overview of the fundamental

principles governing sound barriers and their crucial role in noise mitigation.

1.2.2.2. Introduction to Sound Barriers:

In the midst of urbanization and industrialization, noise pollution has become a ubiquitous challenge, prompting the development of effective countermeasures. Sound barriers, as key components in this endeavour, play a crucial role in mitigating the impact of environmental noise. This section provides a detailed exploration of sound barriers, their intrinsic purpose, and the dynamic evolution they have undergone over time.

Sound barriers are purposeful infrastructural components strategically designed to impede the transmission of sound waves originating from noise sources. Their primary function is to mitigate the impact of environmental noise, serving as a shield that protects specific areas or individuals from undesirable auditory stimuli.

The historical evolution of sound barriers is a narrative that spans from rudimentary implementations to sophisticated contemporary solutions. Early attempts at noise reduction primarily involved basic physical barriers. However, technological advancements in material science, engineering, and acoustics have propelled the development of more nuanced and effective sound barrier technologies.

At its core, the primary role of sound barriers is to act as physical obstacles that alter the propagation path of sound waves. By strategically positioning these barriers, the intensity of noise reaching specific areas or individuals is reduced, thereby mitigating the adverse effects of environmental noise. Beyond noise reduction, sound barriers significantly contribute to preserving the quality of life in urban and suburban environments. By safeguarding residential, commercial, and recreational spaces from excessive noise, these barriers play a pivotal role in enhancing the overall well-being of communities. Early attempts at noise abatement involved the use of basic physical barriers, often with limited efficacy. These early solutions laid the groundwork for subsequent advancements in sound barrier technology.

Modern implementations consider not only effectiveness but also aesthetic and environmental factors. Technological progress in material science, engineering principles, and acoustics has propelled the development of more sophisticated sound barrier solutions.

1.2.2.3. Mechanisms of Noise Mitigation:

Understanding the mechanisms employed by sound barriers is crucial for grasping their functional significance in noise mitigation. One primary mechanism involves the use of materials with acoustic absorption properties, converting sound energy into heat through

frictional processes. Additionally, reflective surfaces and angles influence the reflection of sound waves back towards the noise source. Sound barriers also employ diffraction mechanisms, causing sound waves to bend around or over the barrier, with the degree influenced by height, shape, and frequency. Furthermore, the concept of transmission loss measures the reduction in sound energy passing through a barrier, and insulation effectiveness is evaluated based on preventing sound transmission to the protected side. Some barriers incorporate resonance control mechanisms and vibration-damping materials to counter specific frequencies and minimize vibrational energy transfer. Considering psychoacoustic principles is also essential, as the psychological impact of visually appealing barriers can influence perceived noise reduction. Emerging technologies include adaptive sound barriers equipped with sensors and actuators, dynamically adjusting their properties in real-time to optimize noise reduction based on changing conditions.

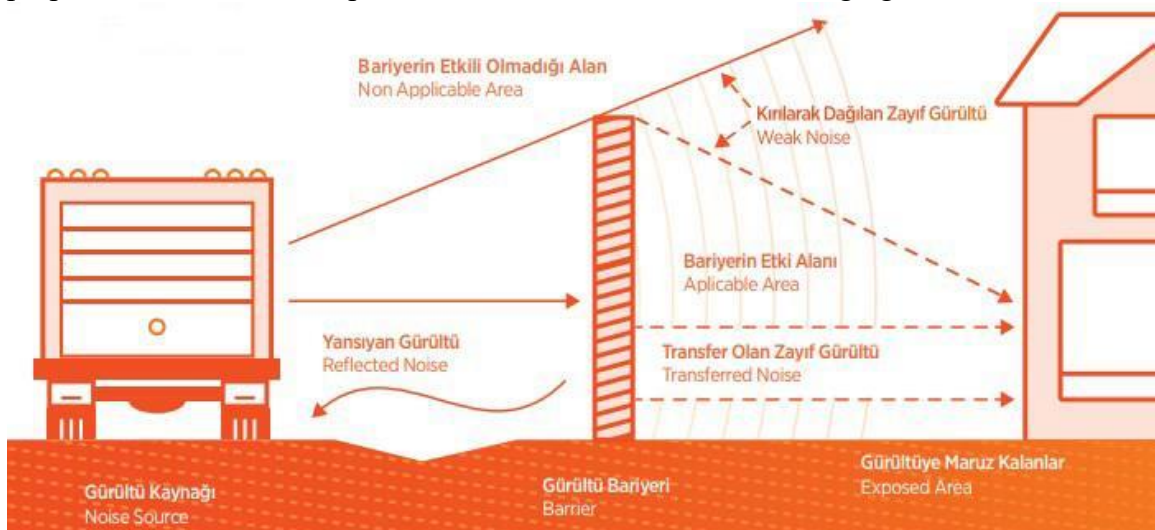


Figure 1.1 Basic representation of noise barrier effect

The basic working principle of sound barriers lies in their ability to obstruct, absorb, reflect, or diffract sound waves, thereby reducing the transmission of noise from a source to a specific area. (Figure 1.1) These barriers leverage fundamental principles of acoustics to mitigate the impact of environmental noise. Here are the key aspects of their basic working principle:

- Absorption: Sound barriers often incorporate materials with acoustic absorption properties. These materials dissipate sound energy by converting it into heat through frictional processes, reducing the intensity of sound waves that pass through.
- Reflection: Reflective surfaces on sound barriers redirect a significant portion of incoming sound waves back towards the noise source. The design of the barrier, including angles and material properties, influences the extent of sound wave reflection.
- Diffraction: Sound barriers disrupt the propagation path of sound waves, causing

them to bend around or over the barrier. The degree of diffraction is influenced by the height, shape, and frequency of the incident sound waves.

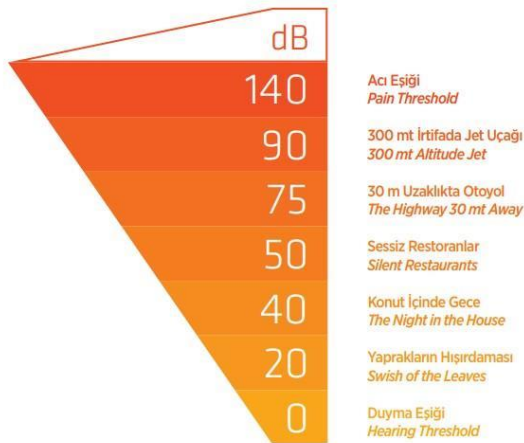


Figure 1.2 Sound level as dB

Transmission Loss and Insulation: Sound barriers aim to achieve transmission loss by reducing the amount of sound energy passing through the barrier. Insulation effectiveness is measured by how well a barrier prevents the transmission of sound to the protected side.

d) **Resonance and Vibration Control:** Some sound barriers incorporate mechanisms to control resonance at specific frequencies. Vibration-damping materials are often used to minimize the transfer of vibrational energy, reducing structure-borne noise.

In essence, sound barriers act as physical obstacles strategically placed to intercept and alter the path of sound waves, thereby diminishing the intensity of noise reaching specific areas or individuals. The selection of materials, barrier design, and consideration of acoustic principles collectively contribute to the overall effectiveness of sound barriers in mitigating environmental noise.

1.2.3. Material of Sound Barriers:

Sound barriers are of critical importance in terms of material selection and design features. The effectiveness of these barriers is directly related to the acoustic properties, density, elasticity, and overall architectural features of the material used.

Material selection: Among the materials used in sound barriers are wood, metal, concrete, glass wool, and acoustic panels. Wood is preferred due to its natural sound absorption properties, while materials like metal and concrete are known for their high reflection characteristics. Glass wool is commonly used for its sound absorption ability. The most common materials for metallic sound barriers are aluminium and galvanized steel.

Material properties: Density: The density of sound barriers affects their capacity to block the passage of sound. Materials with high density generally provide more effective sound insulation. Elasticity: The elastic properties of sound barriers determine the material's ability to absorb or control the transmission of sound waves. Acoustic properties: Features such as the material's acoustic absorption coefficient, reflection coefficient, and transmission loss are crucial in determining the performance of sound barriers.

An emerging trend in the material selection for sound barriers is the use of recycled plastics, as highlighted in the study by Saadeghvaziri and Macbain. Their research proposes an innovative noise wall design that leverages recycled plastic materials and employs a multilayering approach to enhance both stiffness and acoustic performance. The prototypes of this design were rigorously tested, revealing that the transmission loss was on par with conventional materials. This suggests that recycled plastics can be an effective alternative for sound barriers. Additionally, finite element analyses and a specialized analytical model demonstrated that these recycled materials could structurally support increased spans between posts, potentially leading to more cost-effective solutions compared to traditional designs. This advancement not only presents an eco-friendly option by repurposing waste materials but also shows promise in meeting the technical requirements for effective sound insulation.

Design factors: Surface geometry: The surface design of sound barriers affects their ability to absorb or reflect sound waves. Flat surfaces tend to reflect, but various shapes and patterns can contribute to sound absorption. Modular design: Sound barriers are often designed modularly, allowing scalability according to different application needs. Connection and mounting systems: The effectiveness of barriers depends on proper installation and compatibility with the surrounding structures. The material selection and design of sound barriers should be carefully planned according to the specific requirements of the project and environmental factors. This ensures optimal acoustic performance and visual harmony of the barrier.

In alignment with the findings presented by May and Osman in their study on highway noise barriers, it's evident that surface geometry, modular design, and connection systems play pivotal roles in optimizing the effectiveness of such barriers (May & Osman). Their investigation into various barrier designs, including thin, wide, T-profiled, and others, highlights the nuanced relationship between design features and acoustical performance in typical highway scenarios. Importantly, their research emphasizes the impact of barrier configurations on noise reduction, particularly noting the effectiveness of wide top barriers, especially those with T-profiles, and the benefits of absorptive treatments in mitigating sound increases and performance degradation in specific highway configurations. This underscores the importance of integrating design principles with empirical testing to develop sound barriers that not only meet acoustical requirements but also address practical considerations for installation and compatibility with surrounding structures. By

incorporating these insights into the planning and design process, stakeholders can achieve optimal acoustic performance and visual integration, ultimately contributing to more effective noise mitigation strategies on highways.

1.2.3.1. Applications of Sound Barriers:

Sound barriers are widely used in various application areas where effective sound control is needed. These application areas encompass various sectors where sound barriers are adapted to provide effective noise control.

a) Highway sound barriers:

In densely populated areas, highway sound barriers are used to reduce environmental noise and protect nearby residences. They enhance environmental comfort by reducing noise caused by high-density traffic.

b) Railway sound barriers:

Along railway lines, sound barriers are constructed to control the noise generated by train traffic. These barriers are crucial for protecting environmentally sensitive areas and residences from railway noise.

c) Airport sound barriers:

Around airports, airport sound barriers are used to reduce noise from aircraft engines and other air traffic sources. These barriers are planned to protect communities around the airport and minimize noise pollution.

d) Sound barriers for industrial facilities:

Industrial facilities can often generate high noise levels. Sound barriers control the noise around industrial areas, ensuring the protection of surrounding areas.

e) Residential buildings and commercial structures:

Sound barriers are used in residential areas or commercial spaces to prevent the leakage of indoor sounds. This enhances comfort in structures such as residential buildings, hotels, office buildings, and shopping centres.

The diverse application areas of sound barriers emphasize their use in various projects aimed at sound control to enhance environmental sustainability and quality of life. Here is some examples of sound barriers in the sector.

1.2.4. Trapezoidal Sound Barriers: Design, Performance, and Applications:

Trapezoidal sound barriers represent a distinct category within sound mitigation structures, characterized by their unique trapezoidal configuration. This design is defined by its tapered appearance, where one side of the barrier is notably shorter than the opposite side, giving it a trapezoid-like silhouette. This specialized shape is not merely aesthetic but is tailored to enhance the barrier's effectiveness in sound deflection and absorption, making it a significant choice for various noise control applications.



Figure 1.3 Trapez model view of noise barrier

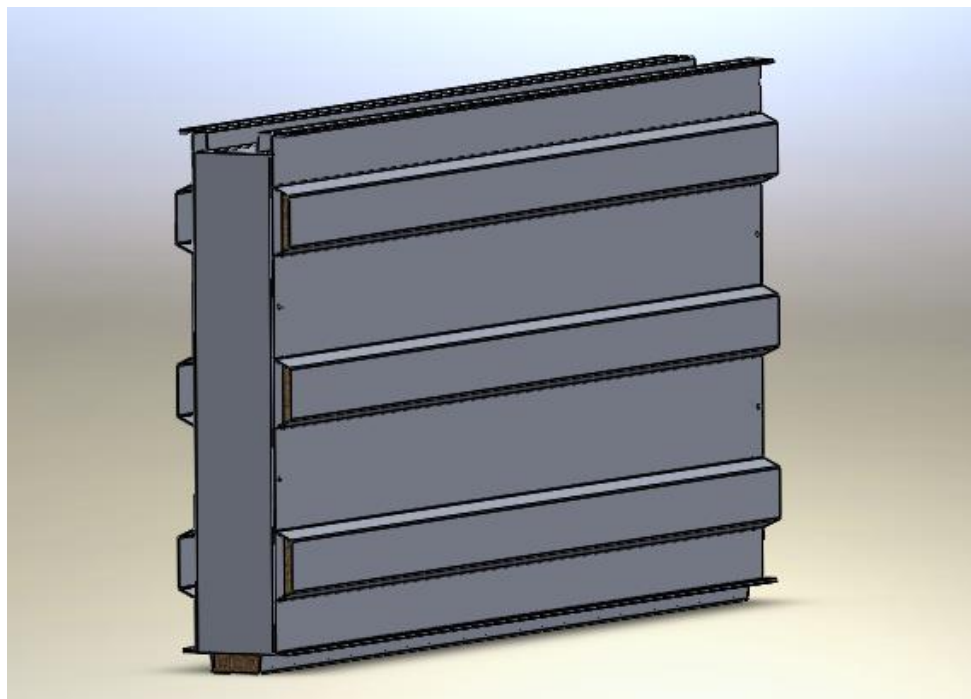


Figure 1.4 CAD drawing of trapezoidal noise barrier.

1.2.5. Droplet Model for Sound Barriers: Aesthetic and Acoustic Advancements:

The Droplet Model for sound barriers embodies a groundbreaking fusion of aesthetic appeal and acoustic innovation. Drawing inspiration from the natural form and characteristics of droplets, this model is designed to elevate noise control solutions by integrating visual elegance with cutting-edge sound attenuation capabilities. It aims not just to mitigate noise but to do so in a way that enhances the visual landscape, offering a harmonious blend of functionality and design.

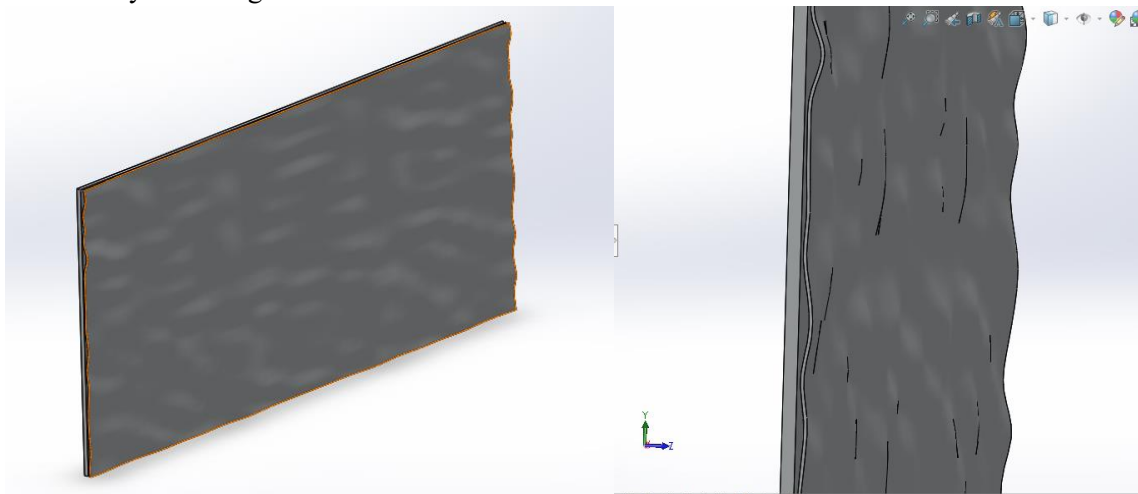


Figure 1.5 Droplet Model view 1

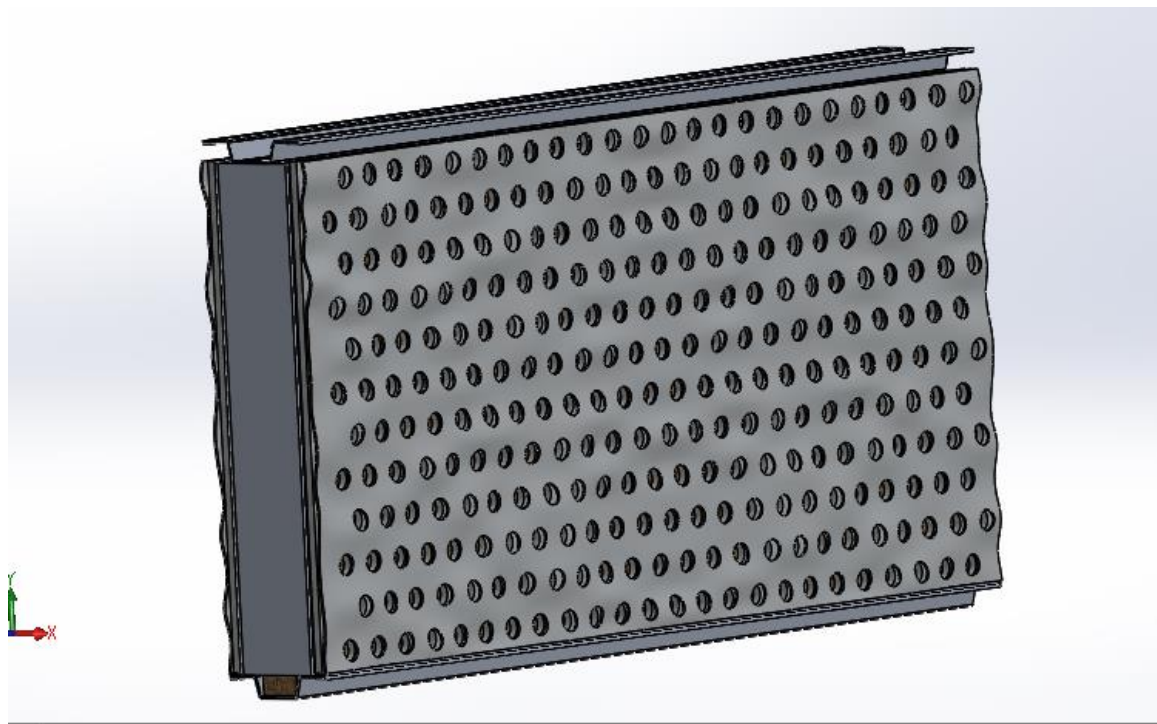


Figure 1.6 Droplet Model view 2

2. ANALYSIS CALCULATIONS BACKGROUND

Within the scope of this research, acoustic structure relationship and sound transmission loss values will be analysed comparatively for two different designs. In the first part of the study, mathematical principles based on acoustic structure analysis will be discussed in detail. In this context, the effects of sound on structures, mathematical modelling and calculation of acoustic properties will be discussed.

Then, the analysis methodology using COMSOL Multiphysics software will be explained in detail. COMSOL Multiphysics is a software platform capable of simulating multiple physical domains and solving complex problems such as acoustic structure analysis. In this chapter, the basic principles of the software, the modules used and the analysis process will be examined step by step and how it can be used to obtain accurate results for acoustic structures will be explained.

2.1. ACOUSTIC-STRUCTURE ANALYSIS

Domain equations:

Within the framework of Pressure Acoustics, the standard approach for simulating harmonic sound waves, particularly in aquatic environments, employs the Helmholtz equation to determine sound pressure dynamics.

$$\nabla \cdot \left(-\frac{1}{\rho_c} \nabla p \right) - \frac{\omega^2 p}{\rho_c \cdot c_c^2} = 0 \quad (3.1)$$

In this equation, "p" represents pressure, measured in Newtons per square meter (N/m^2), while " ρ_c " stands for the fluid's density, with units of kilograms per cubic meter (kg/m^3). The symbol " ω " denotes angular frequency, expressed in radians per second (rad/s), and " c_c " indicates the speed of sound, in meters per second (m/s). It's important to note that both the density and the speed of sound can assume complex values (indicated by the subscript "c"), which is essential for accurately modelling fluids that exhibit energy dissipation. However, in the context of this specific model, these variables are considered to have real values due to the absence of modelled damping effects.

Table 2-1 Acoustics Domain Data

| Quantity | Value | Description |
|-------------------|------------------------|----------------|
| ρ_c | 1.293 kg/m^3 | Density of air |
| c_c | 1500 m/s | Speed of sound |
| $f = \omega/2\pi$ | 60 kHz | Frequency |

Boundary Conditions:

For the outer boundary of the air domain, an incident plane wave is introduced to simulate an approaching sound wave. Concurrently, a spherical wave, generated in response by the cylinder, is permitted to exit the system. Within the framework of Pressure Acoustics in the Frequency Domain interface, this setup is achieved through the application of the Spherical Wave Radiation boundary condition. This particular boundary condition is advantageous for scenarios where the external environment acts as an extension of the domain itself. The direction of the incident wave, denoted as k , is determined by two angular parameters, θ and Φ , with θ ranging from 0 to π and Φ from 0 to 2π . The parameters for this incident wave are detailed under the Incident Pressure Field feature.

Table 2-2 Radiation Boundary Condition Settings

| Quantity | Value | Description |
|----------|---|--------------------------------|
| k | $(\sin \theta \cos \varphi, \sin \theta \sin \varphi, \cos \theta)$ | Incident wave direction vector |
| p_0 | 1 Pa | Pressure amplitude |

Interface Cylinder-Water

The coupling between the fluid domain (pressure waves) and the solid is automatically done via the Acoustic–Structure Boundary multiphysics coupling. The automatic boundary condition sets the boundary load \mathbf{F} (force/unit area) on the solid cylinder to

$$\mathbf{F} = -\mathbf{n}_s p \quad (3.2)$$

where \mathbf{n}_s is the outward-pointing unit normal vector seen from inside the solid domain. While on the fluid side the normal acceleration experienced by the fluid is set equal to the normal acceleration of the solid. Mathematically this means that

$$-\mathbf{n}_a \cdot \left(-\frac{1}{\rho_0} \nabla p + \mathbf{q} \right) = \mathbf{a}_n \quad (3.3)$$

where \mathbf{n}_a is the outward-pointing unit normal vector seen from inside the acoustics domain, and the normal acceleration a_n is equal to $(\mathbf{n}_a \cdot \mathbf{u})\omega^2$, where \mathbf{u} is the calculated harmonic-displacement vector of the solid structure.

Hard-wallcomparison

Alternatively, for comparative purposes, one might examine a simplified version of the model where the solid boundary is treated as an impenetrable barrier. This means the cylinder remains unaffected by the acoustic waves, yet it influences the distribution of sound within the environment. This effect is modelled by applying a fixed constraint to all

solid interfaces, essentially setting displacement (u) to zero. Consequently, this approach simplifies the original condition to what is termed the sound hard boundary condition, where the normal acceleration (a_n) is also set to zero.

$$n_a \cdot \left(-\frac{1}{\rho_0} \nabla p + q \right) = 0 \quad (3.4)$$

2.2. Sound Transmission Loss Analysis

SOUND TRANSMISSION LOSS(STL)

A key measure for evaluating a material's effectiveness in sound insulation is the Sound Pressure Transmission Loss (STL), also referred to as the sound reduction index. While the specifics of its computation will be elaborated upon in subsequent sections, fundamentally, STL quantifies the disparity between incident and transmitted sound pressures. The STL value for a barrier is influenced by its material composition and structural design, varying across different frequencies. The primary determinant of STL across a spectrum lies in the frequency-specific response, which allows for the categorization of the STL profile into four distinct frequency-based regions, as outlined in the sections that follow.

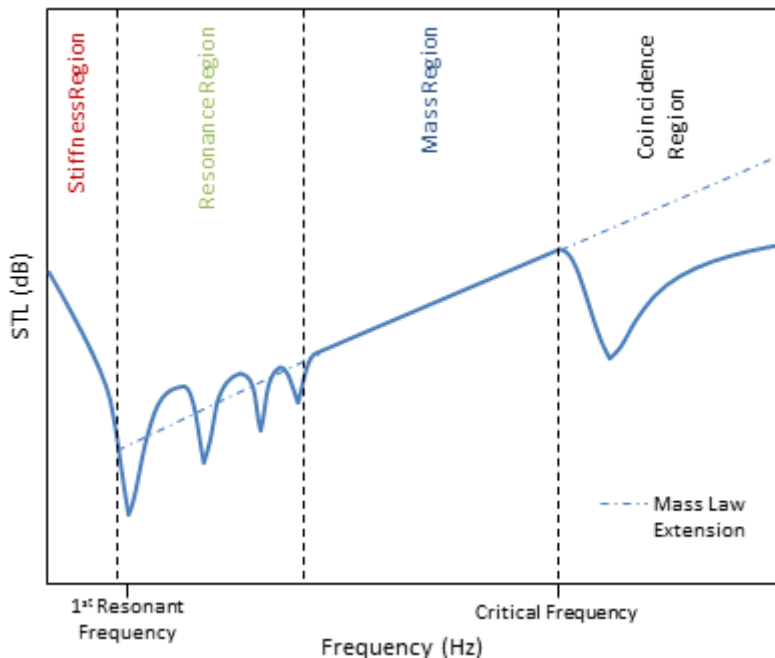


Figure 2.1 Frequency dependent sound transmission regions of a panel

In the lower frequency spectrum, the stiffness of the panel primarily dictates the Sound Transmission Loss (STL), with damping and mass playing minimal roles. Within this bandwidth, an increase in STL is noted alongside an elevation in the panel's first resonance frequency, culminating at the onset of this resonance. As frequencies ascend slightly above this threshold, the panel's natural resonances take precedence in influencing STL. These

resonances, indicative of heightened panel vibrations, are determined by the panel's material, dimensions, and installation specifics. The interaction with these resonant frequencies results in significant sound energy transfer across the panel, manifesting as marked reductions in STL.

Progressing beyond the resonance domain, the panel's STL enters the mass-controlled region, crucial for numerous sound insulation endeavours. It is in this domain that the mass law comes into play, offering a precise STL estimation based on the panel's mass.

$$STL = 10 \log \left[1 + \left(\frac{m\omega \cos \theta}{2\rho c} \right)^2 \right] \quad (3.5)$$

m denotes the mass per unit area, ω signifies the angular frequency, θ is the incident angle, ρ represents the density of the acoustic medium, and c is the velocity of sound within the acoustic medium. For waves that are normally incident, the angle of incidence is 0° . By substituting this angle into the equation, converting the angular frequency to cyclic frequency (where $\omega/2\pi=f$), and assuming that $m\omega/(2\rho c) \gg 1$, the mass law can be simplified to the normal incidence mass law.

$$STL = 20 \log(fm) - 42 \text{ dB} \quad (3.6)$$

where f is the cyclic frequency in Hertz and m is the mass per unit area. While Eq. 1.2 is an empirical law, it accurately describes sound transmission in the mass region and provides a rough estimate for sound transmission in the resonance region. At even higher frequencies, bending waves can cause the phenomenon known as the coincidence effect. The coincidence effect first appears at the critical frequency (f_c) of the panel, which is given by:

$$f_c = \frac{c^2}{1.8h} \sqrt{\frac{\rho}{E}} \quad (3.7)$$

In this formula, "c" represents the speed of sound within the material, " ρ " denotes the material's density, and "E" signifies the material's elastic modulus. The coincidence effect emerges when the wavelengths of the bending waves within the barrier align with those of the incoming sound waves. Such alignment ensures that the bending movement of the barrier synchronizes with the surface movements of the panel. This synchronization facilitates a heightened transfer of sound energy from the incident waves to the other side of the panel, leading to a significant reduction in Sound Transmission Loss (STL), a phenomenon often described as the coincidence dip, commencing at the critical frequency. This specific frequency range is identified as the coincidence region.

The STL through a building component, like a door, a window, a wall segment, or a sound insulation structure, is defined as the ratio expressed in dB of the total incident power P_{in} on the structure relative to the total transmitted power P_{tr}

$$STL = 10 \log_{10} \left(\frac{p_{in}}{p_{tr}} \right) \quad (3.8)$$

STL measurements are calibrated under the assumption of a diffuse acoustic environment on the source side. There are established standards for STL assessment, such as ASTM E90 and ISO 10140, all designed to either directly or indirectly quantify the power of both incident and transmitted sound waves. A prevalent methodology employed is known as the two-room technique. This approach typically involves a reverberation chamber on the source end. Depending on the setup, the receiving end may also feature a reverberation room (creating a reverberant-reverberant configuration) or, alternatively, an anechoic chamber (resulting in a reverberant-anechoic setup). Illustrations of these setups are provided in Figure 8 for visual reference.

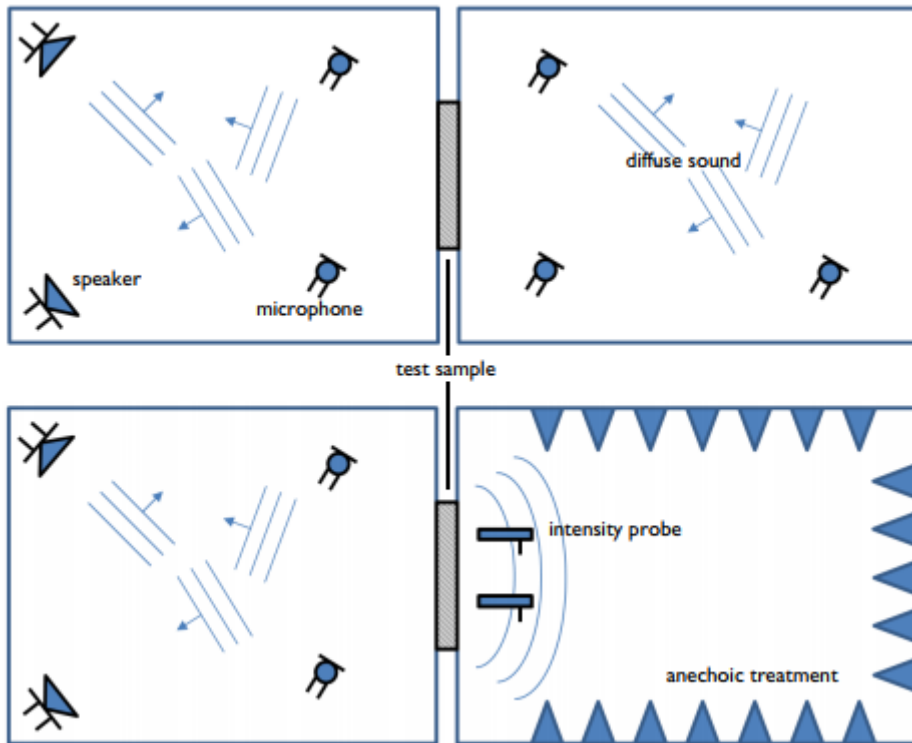


Figure 2.2 The two variations of the two-room configuration for measuring the sound transmission loss. Top: source and receiver reverberation rooms. Bottom: source reverberation room and receiver anechoic room.

In both cases, the incident power on the source side is computed as

$$P_{in} = \frac{p_{rms}^2}{4\rho_0 c_0} S_s \quad (3.9)$$

where S_s is the area of the test surface on the source side (the area of the concrete wall tested), p_{rms} is the RMS pressure in the source room, ρ_0 is the air density, and c_0 is the speed of sound in air. This expression is derived by considering the incident power on a surface in an ideal diffuse acoustic field, see Ref. 1 and Ref. 2.

The expressions used to compute the incident and transmitted power for the reverberant

case are only valid as long as the acoustic field is diffuse. A measure for the upper limit of modal behaviour is given by the Schroeder frequency

$$f_s = 2000 \sqrt{\frac{T_{60}}{V}} \quad (3.10)$$

where V is the room volume and T_{60} is the reverberation time; see Ref. 1. A room of volume V is said to be acoustically large when the studied frequency f is larger than the Schroeder frequency, giving the condition

$$V > \left(\frac{2000}{f}\right)^2 T_{60} \quad (3.11)$$

Reverberant-Reverberant Setup

In the setup where the receiver room is a reverberation room (Figure 1 top) and the sound field is assumed to diffuse, the transmitted power is given by

$$P_{tr} = \frac{p_{rms}^2}{4\rho_0 c_0} Ar \quad Ar = \sum_i s_i a_i \quad (3.12 \text{ a,b})$$

where p_{rms} is the RMS pressure in the receiver room and Ar is the receiver room absorption area, that is, the sum of products between each surface area S_i and its absorption coefficient α_i . The expression stems from an energy balance consideration where the total absorbed energy is equal to the radiated energy of the source. Combining Equation 2 and Equation 5 give the expression for the STL for the reverberant-reverberant setup

$$STL = SPL_s - SPL_r + 10 \log_{10} \left(\frac{s_s}{Ar} \right) \quad (3.13)$$

where SPLs and SPLr are the average sound pressure levels in the source and the receiver room, respectively. Averaging is done on the squared pressure before transforming to the dB scale.

Note that a correction to Equation 5 is sometimes introduced based on the Waterhouse expression. In a room with a diffuse field, the RMS pressure at the walls will be larger by a factor 2 because each incident wave is coherent with its corresponding reflected wave, see Ref. 2. The corrected expression reads

$$P_{tr} = \frac{\rho_{(rms)}^2}{\rho_0 c_0^2} V_r \left(1 + \frac{s_r \lambda}{8V_r}\right) \frac{13.8}{EDT} \quad (3.14)$$

where EDT is the early decay time, V_r is the receiver room volume, S_r the receiver room surface area, and λ is the wavelength.

Reverberant-Anechoic Setup

In the reverberant-anechoic configuration (Figure 1 bottom), the transmitted power is directly measured on the receiver side using an intensity probe. The measurement is performed in several locations in front of the test element and averaged. The transmitted power is then simply given by

$$P_{tr} = S_r I_{tr} \quad (3.15)$$

combining this expression with Equation 1 and Equation 2 gives

$$STL = SPL_s - SPL_r + 10 \log_{10} \left(\frac{S_s}{S_r} \right) - 6.14 \quad (3.16)$$

SIL_{tr} is the transmitted sound intensity level, and for flat samples $S_s = S_r$. The numeric constant stems directly from the definitions of SPL and SIL and the equations for the power, it is expressed as

$$10 \log_{10} \left(\frac{1}{4} \frac{(p_{ref})^2}{I_{ref}} \frac{1}{\rho_0 c_0} \right) \approx -6.14 \quad (3.17)$$

where $p_{ref} = 20 \mu\text{Pa}$, $I_{ref} = 10-12 \text{ W/m}$, $\rho_0 = 1.2 \text{ kg/m}^3$, and $c_0 = 343 \text{ m/s}$.

When simulating the STL it is preferable to avoid modelling the source and receiver rooms as this would be computationally extremely expensive. Instead, the setup is based on assuming an ideal diffuse field on the source side and an ideal anechoic termination on the receiver side of the test sample. The model also assumes that the test sample has little influence on the sound field on the source side. This is true for relatively stiff structures with low acoustic absorption properties. This is the case for the concrete wall studied in this example. The sound field on the source side can then be defined as a sum of $2N$ uncorrelated plane waves moving in random directions. It can also be assumed that one-half of these waves travel in the negative x direction and the other half in the positive x direction. Knowing that the concrete wall is located in the $x = 0$ plane, only the waves travelling in the positive x direction contribute to the incident pressure on the wall surface. The source room pressure field travelling in the positive x direction is then

$$p_{x,r_{00}m} = \frac{A}{\sqrt{2N}} \sum_{n=1}^N \exp(-i(k_{n,x} x + k_{n,y} y + k_{n,z} z)) \exp(i \cdot \phi_n) \quad (3.18)$$

$$\begin{aligned} k_{n,x} &= \cos(\theta_n) \\ k_{n,y} &= \sin(\theta_n) \cos(\varphi_n) \\ k_{n,z} &= \sin(\theta_n) \sin(\varphi_n) \end{aligned}$$

(3.19 a,b,c)

where the polar angles $0 \leq \theta_n \leq \pi/2$ and $0 \leq \varphi_n \leq 2\pi$ as well as the phase $0 \leq \Phi_n \leq 2\pi$ are independent random numbers and A is the amplitude of the plane waves; φ_n and Φ_n are taken directly from uniform distributions, whereas θ_n is obtained as $\theta_n = \arccos(q_n)$, q_n being a random variable with a uniform distribution between 0 and 1. This ensures a uniform distribution of wave numbers over the desired hemisphere. In the model, a new set of random numbers is generated for each n in the sum. The term ensures that the field has a constant intensity for any choice of N . Because the plane waves are uncorrelated, the total mean square pressure in the source room is $prms2 = |2px,room|^2/2$, with the term $2px,room$ accounting for the total diffuse field (positive and negative x directions). The theoretical limit for large N of the mean square pressure in the room (away from walls) is $prms,th2 = |A|^2/2$.

The concrete wall is located at $x = 0$, where the incident diffuse field is reflected. The reflected component of the field is

$$p_{refl} = \frac{A}{\sqrt{2N}} \sum_{n=1}^N \exp(-i(-k_{n,x} x + k_{n,y} y + k_{n,z} z)) \exp(i \cdot \phi_n) \quad (3.20)$$

The reflected field is coherent with the incident field, as discussed for Equation 5. At the surface of the concrete wall, the total pressure load applied to the structure is the sum of the incident and reflected pressures:

$$p_{wall} = p_{x,room} + p_{(refl)} \quad (3.21)$$

3. ANALYSIS METHOD, SETUP AND RESULTS

The analysis will be conducted using COMSOL Multiphysics software, version 6.2, which is renowned for its advanced simulation capabilities in the field of acoustics. Both the trapezoidal and droplet (waterdrop) models will be subjected to this rigorous computational analysis.

In the simulation setup, a random noise environment will be created over the same frequency range for both models to assess their Sound Transmission Loss (STL) values and other relevant acoustic parameters. This randomized approach aims to emulate a broad spectrum of sound frequencies to ensure that the STL analysis captures a realistic and comprehensive range of scenarios that the barriers might encounter in an actual setting.

Once the acoustic simulations are complete, we will perform a detailed comparative analysis of the STL results for both models. This step is crucial to understand the relative strengths and weaknesses of each design in various frequency bands. By comparing these results, we can identify which design performs better under specific conditions and why.

Following the comparative analysis, the next phase will involve a critical examination of the trapezoidal model's SRI values derived from the simulation against the certified test results obtained by TSE (Turkish Standards Institution). This juxtaposition will help validate the accuracy of our simulation models and reveal any discrepancies. It will also allow us to refine our simulation parameters if necessary, ensuring that our computational predictions align closely with empirical evidence from standardized tests.

This iterative process of analysis, comparison, and refinement is an integral part of the engineering design and optimization cycle. It ensures that the final product not only meets the required standards but also performs optimally in its intended environment. Through this meticulous approach, we strive to deliver sound barrier designs that are not only theoretically sound but also practically effective.

3.1. EXPERIMENTAL ANALYSIS SETUP

3.1.1. Global Definitions

| | |
|---------|---|
| Name | STLsade49.mph |
| Path | C:\Users\LENOVO\Desktop\Engineering Project\STLsade49.mph |
| Version | COMSOL Multiphysics 6.2 (Build: 290) |

USED PRODUCTS

| |
|---------------------|
| Acoustics Module |
| CAD Import Module |
| COMSOL Multiphysics |

Design Module

COMPUTER INFORMATION

| | |
|------------------|---|
| CPU | Intel64 Family 6 Model 142 Stepping 12, 4 cores, 7.7 GB RAM |
| Operating system | Windows 10 |

3.1.1.1. Parameters

(This part same for both analyses.)

Table 3-1 Parameters table

| Name | Expression | Value | Description |
|------|-------------|-----------------------|-------------------------------|
| T | 6[mm] | 0.006 m | Thickness |
| H | 0.5[m] | 0.5 m | Height |
| W | 1[m] | 1 m | Width |
| seed | 42 | 42 | Seed for random function |
| N | 100 | 100 | Number of random waves in sum |
| c0 | 343.2[m/s] | 343.2 m/s | Speed of sound in air |
| rho0 | 1.2[kg/m^3] | 1.2 kg/m ³ | Density of air |
| fmax | 4000[Hz] | 4000 Hz | Maximum study frequency |
| m | 15[kg/m^2] | 15 kg/m ² | Wall surface density |
| A | 1[Pa] | 1 Pa | |
| n | 1 | 1 | |

3.1.1.2. Functions

(This part same for both analyses.)

Random 1

| | |
|---------------|--------------|
| Function name | costheta_rnd |
| Function type | Random |

Random 2

| | |
|---------------|---------|
| Function name | phi_rnd |
| Function type | Random |

Random 3

| | |
|---------------|-----------|
| Function name | phase_rnd |
| Function type | Random |

Integration 1

| | |
|---------------|-------------|
| Coupling type | Integration |
| Operator name | intop_in |

Interpolation 3

| | |
|----------------|---------------|
| Function names | STL_typical |
| Function type | Interpolation |

3.1.1.3. Variable

(This part same for both analyses.)

Table 3-2 Variables

| Name | Expression | Unit | Description |
|-----------|--|----------------|---|
| phi | phi_rnd(n, freq[1/Hz], 1, seed) | | |
| theta | acos(costheta_rnd(n, freq[1/Hz], 2, seed)) | rad | |
| phase | phase_rnd(n, freq[1/Hz], 3, seed) | | |
| kx | cos(theta)*k0 | 1/m | Partial wave vector, x-component |
| ky | sin(theta)*cos(phi)*k0 | 1/m | Partial wave vector, y-component |
| kz | sin(theta)*sin(phi)*k0 | 1/m | Partial wave vector, z-component |
| k0 | 2*pi*freq/c0 | 1/m | Propagation constant |
| p_room | 1[Pa]/sqrt(N)*sum(exp(i*phase)*exp(-i*(kx*x + ky*y + kz*z)), n, 1, N) | Pa | Room diffuse field |
| p_refl | 1[Pa]/sqrt(N)*sum(exp(i*phase)*exp(-i*(-kx*x + ky*y + kz*z)), n, 1, N) | Pa | Reflected acoustic field at x=0 |
| p_wall | p_room + p_refl | Pa | Total wall pressure (mechanical load) |
| px_room | A/sqrt(2*N)*sum(exp(i*phase)*exp(-i*(kx*x + ky*y + kz*z)), n, 1, N) | Pa | Room diffuse pressure field, waves in positive x direction |
| vx_room | A/(acpr.omega*rho0)/sqrt(2*N)*sum(kx*exp(i*phase)*exp(-i*(kx*x + ky*y + kz*z)), n, 1, N) | m/s | Room diffuse particle velocity field, waves in positive x direction |
| p_room_sq | 2*abs(px_room)^2 | kg^2/(m^2*s^4) | Room diffuse field, total squared pressure |

| Name | Expression | Unit | Description |
|---------|-------------------------------|-------|--|
| Ix_room | 0.5*realdot(px_room, vx_room) | W/m^2 | Sound intensity, positive x direction |
| P_in | intop_in(Ix_room) | W | Incident power on the concrete surface |

| Name | Expression | Unit | Description |
|------------|---|---|---|
| P_in_proom | $\text{intop_in}(0.5 * \rho_{\text{room}} * \text{sq}) / (4 * \rho_0 * c_0)$ | W | Incident power (room pressure) |
| p_ms_th | $0.5 * A^2$ | $\text{kg}^2 / (\text{m}^2 \cdot \text{s}^4)$ | Theoretical mean square pressure in source room (limit N->infinity) |
| P_in_th | $\text{intop_in}(p_{\text{ms_th}}) / (4 * \rho_0 * c_0)$ | W | Theoretical incident power (limit N->infinity) |
| P_tr | $\text{intop_tr}(\text{acpr.Ix})$ | W | Transmitted power |

3.1.2. Selection

Selection

| | |
|------------------------|--|
| Geometric entity level | Boundary |
| Selection | Geometry geom1: Dimension 2: Boundary 67 |

| | |
|------------------------|---|
| Geometric entity level | Boundary |
| Selection | Geometry geom1: Dimension 2: Boundaries 81–92, 98–100 |

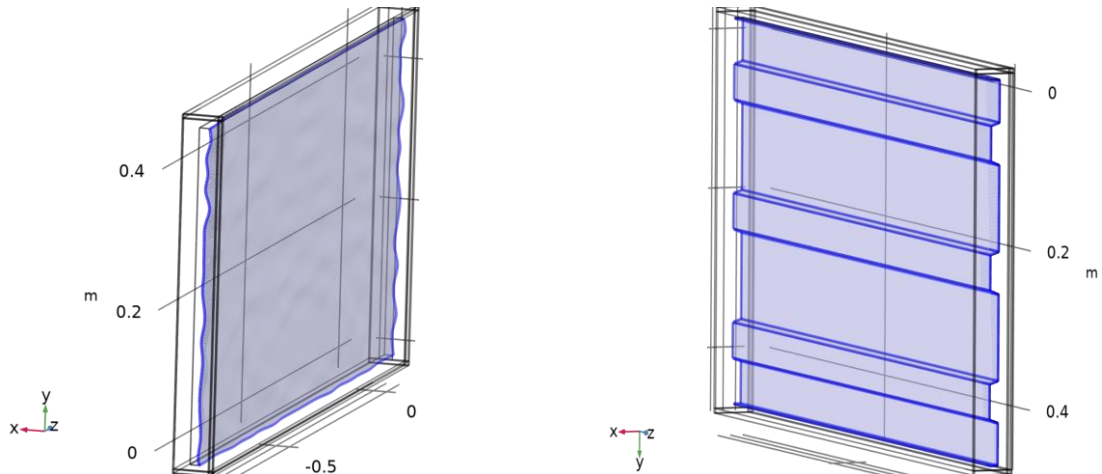


Figure 3.1 Front face selection

Selection
Integration 2

| | |
|---------------|-------------|
| Coupling type | Integration |
| Operator name | intop_tr |

Selection

| | |
|------------------------|--|
| Geometric entity level | Boundary |
| Selection | Geometry geom1: Dimension 2: Boundary 72 |

| | |
|------------------------|---|
| Geometric entity level | Boundary |
| Selection | Geometry geom1: Dimension 2: Boundaries 67–68, 71–80, 94–96 |

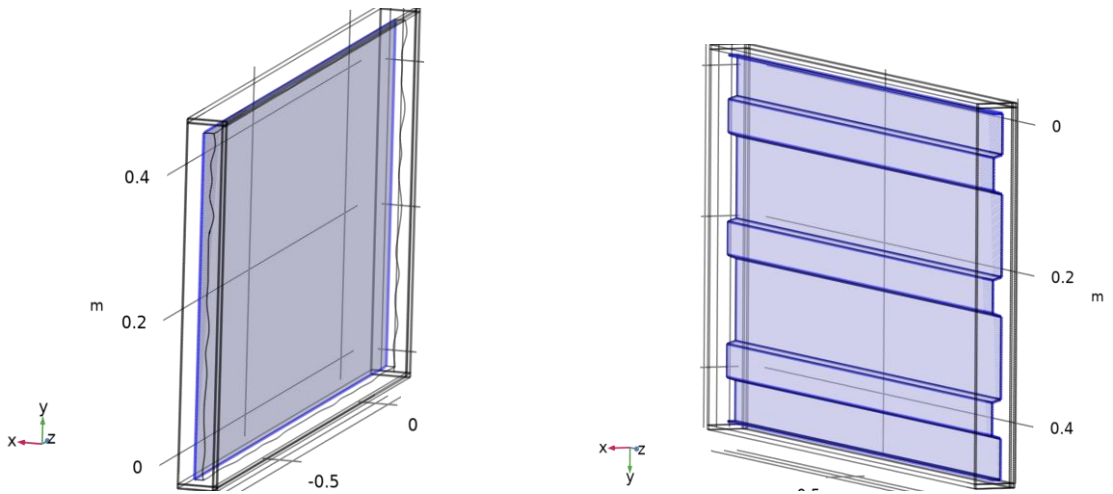


Figure 3.2 Back face selection

3.1.3. Materials and domain

Coordinate Systems

Boundary System 1

| Coordinate system type | Boundary system |
|------------------------|-----------------|
| Tag | sys1 |

Artificial Domains

Perfectly Matched Layer 1

| | |
|-----|------|
| Tag | pml1 |
|-----|------|

Selection

| Geometric entity level | Domain | Domain |
|------------------------|---|--|
| Selection | Geometry geom1: Dimension 3: Domains 1–18 | Geometry geom1: Dimension 3: Domains 1–13, 15–18 |

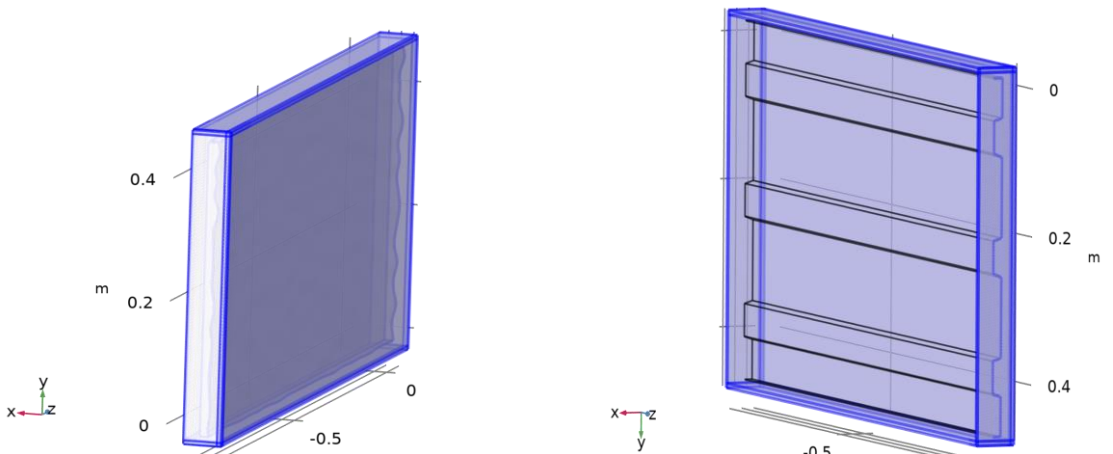


Figure 3.3 Perfectly matched layer selection

Geometry 1

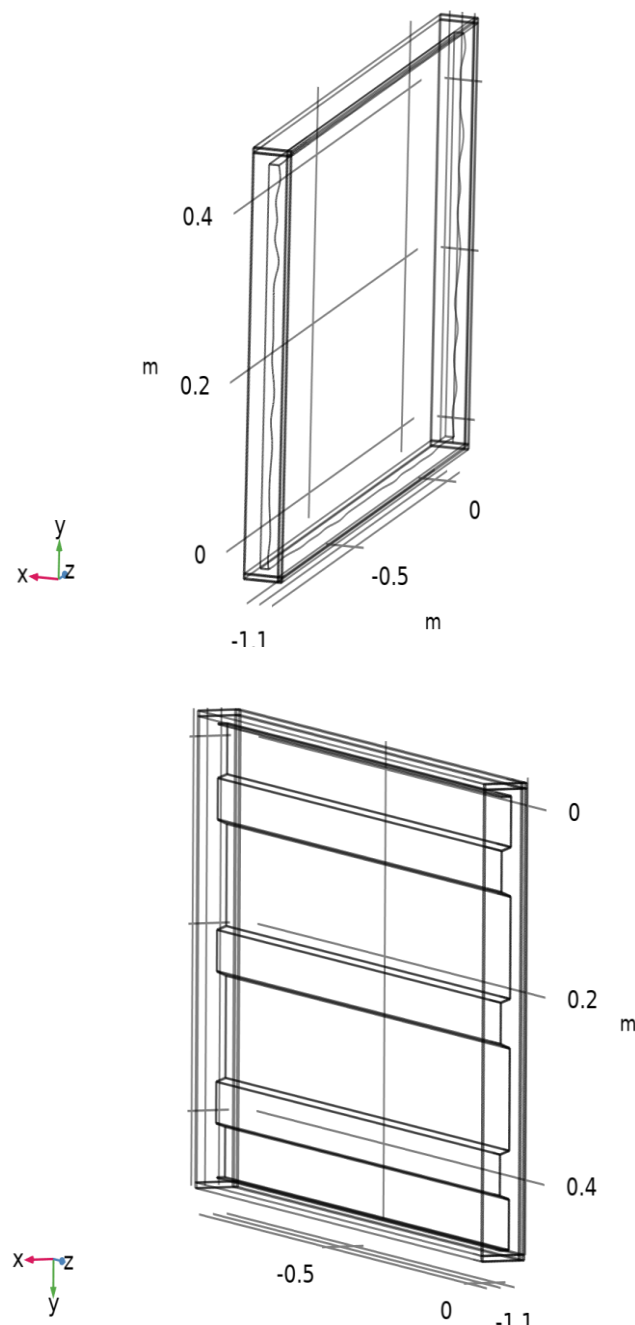


Figure 3.4 Geometry drawing view

Geometry 1
Units

| | |
|--------------|-----|
| Length unit | m |
| Angular unit | deg |

Materials
Air

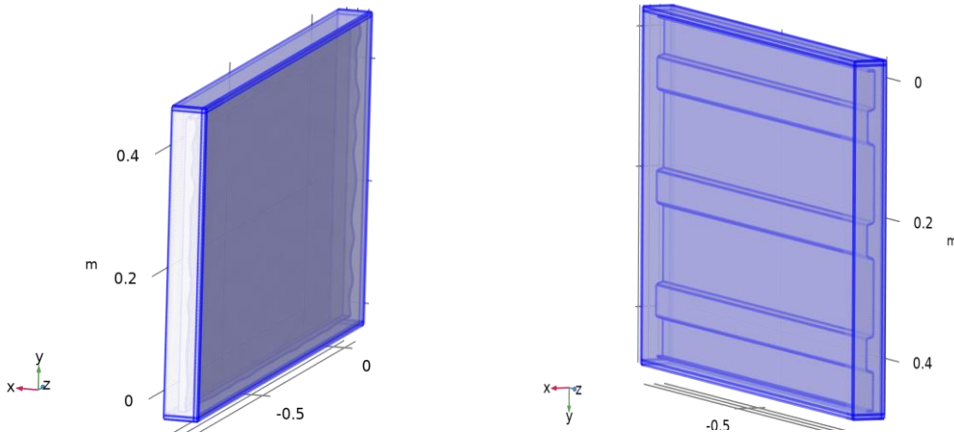


Figure 3.5 Air domain selection

Air Selection

| Geometric entity level | Domain | Domain |
|------------------------|--|--|
| Selection | Geometry geom1: Dimension 3: All domains | Geometry geom1: Dimension 3: All domains |

Aluminum

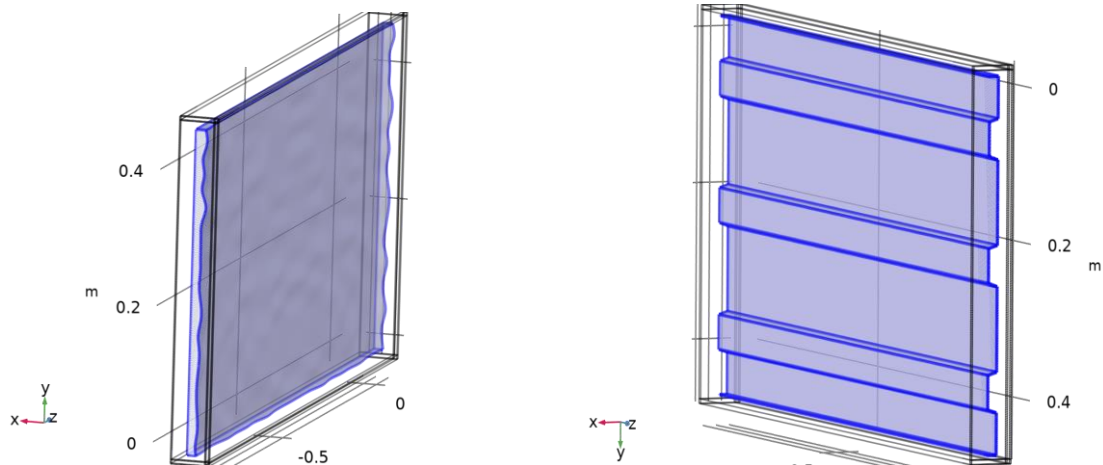


Figure 3.6 Aluminum domain selection

Aluminium Selection

| Geometric entity level | Domain | Domain |
|------------------------|--|--|
| Selection | Geometry geom1: Dimension 3: Domain 19 | Geometry geom1: Dimension 3: Domain 19 |

3.1.4. Pressure Acoustics, Frequency Domain

Pressure Acoustics, Frequency Domain

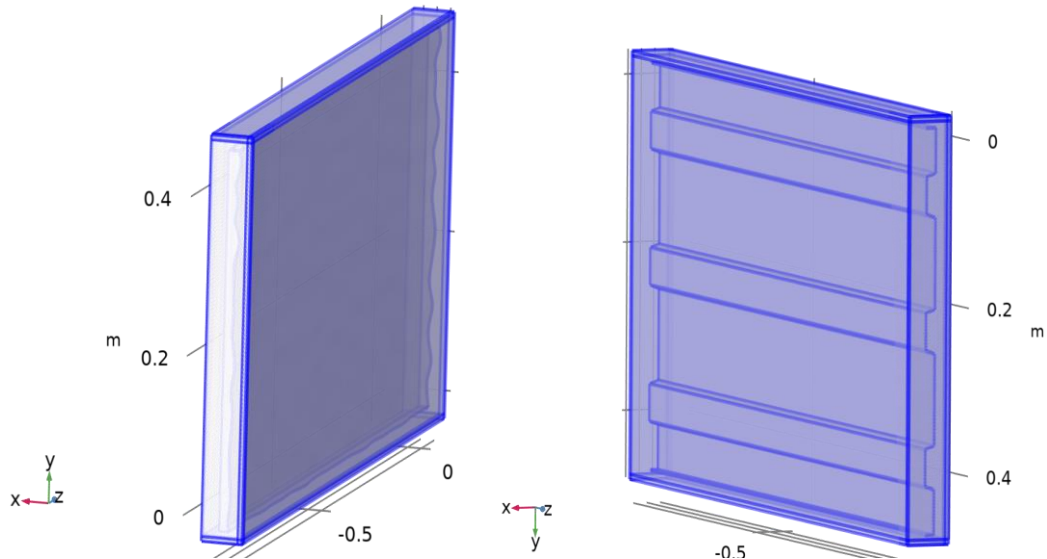


Figure 3.7 Pressure Acoustics, Frequency Domain Selection

Pressure Acoustics, Frequency Domain Equations

$$\nabla \cdot \left(-\frac{1}{\rho_c} (\nabla p_t - \mathbf{q}_d) \right) - \frac{k_{eq}^2 p_t}{\rho_c} = Q_m$$

$$p_t = p + p_b$$

$$k_{eq}^2 = \left(\frac{\omega}{c_c} \right)^2$$

Features

| Name | Level |
|------------------------------|----------|
| Pressure Acoustics 1 | Domain |
| Sound Hard Boundary (Wall) 1 | Boundary |
| Initial Values 1 | Domain |

Solid Mechanics

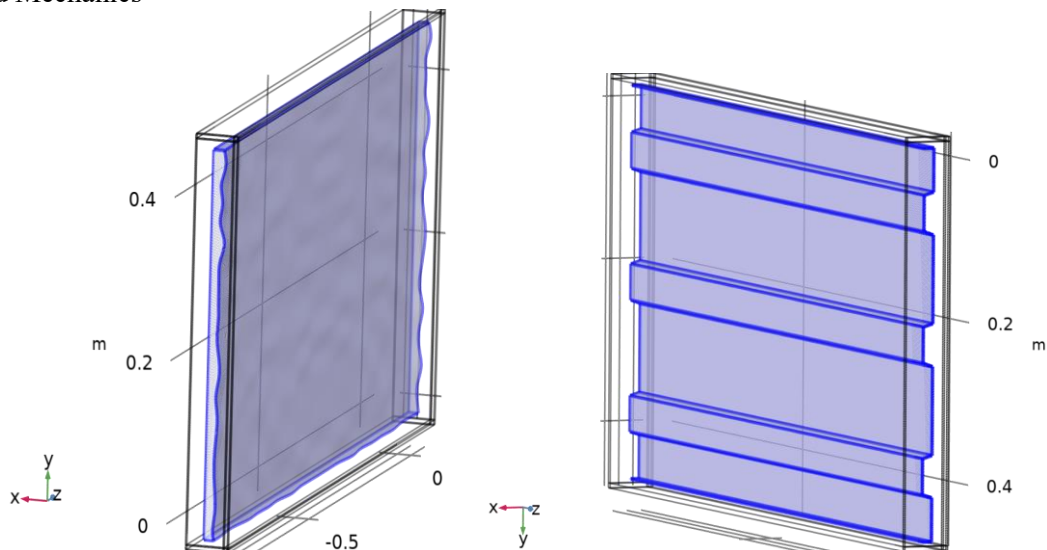


Figure 3.8 Solid mechanics domain selection

Solid Mechanics Equations

$$-\rho\omega^2\mathbf{u} = \nabla \cdot \mathbf{S} + \mathbf{F}_v e^{i\phi}$$

Features

| Name | Level |
|---------------------------|----------|
| Linear Elastic Material 1 | Domain |
| Free 1 | Boundary |
| Initial Values 1 | Domain |
| Fixed Constraint 1 | Boundary |
| Boundary Load 1 | Boundary |

3.1.5. Multiphysics

Multiphysics

Acoustic-Structure Boundary 1

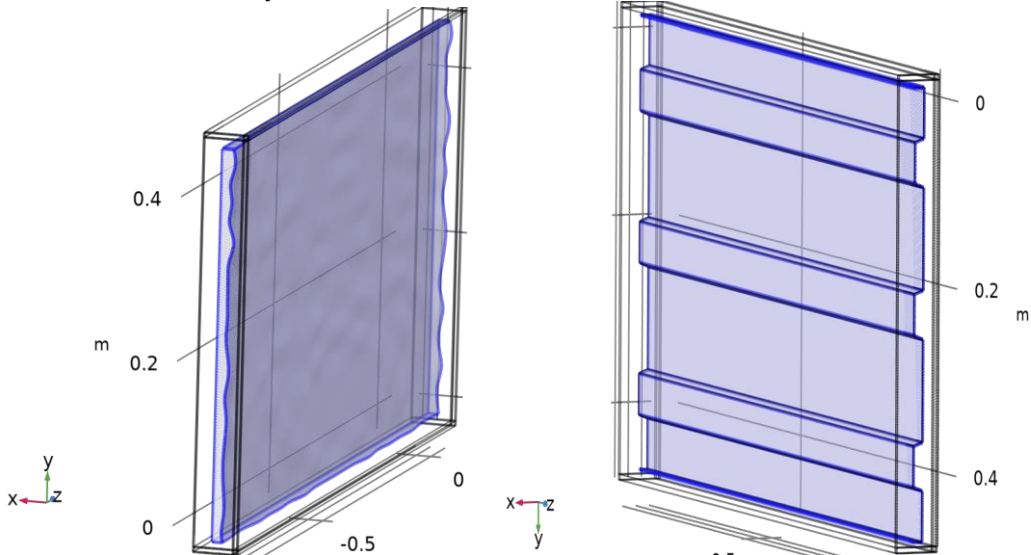


Figure 3.9 Acoustic-Structure Boundary selection

Acoustic-Structure Boundary 1 Equations

Exterior:

$$-\mathbf{n} \cdot \left(\frac{1}{\rho_c} (\nabla p_t - \mathbf{q}_d) \right) = -\mathbf{n} \cdot \mathbf{u}_{tt}$$

$$\mathbf{F}_A = p_t \mathbf{n}$$

Interior:

$$-\mathbf{n} \cdot \left(\frac{1}{\rho_c} (\nabla p_t - \mathbf{q}_d) \right)_{up} = -\mathbf{n} \cdot \mathbf{u}_{tt}$$

$$-\mathbf{n} \cdot \left(\frac{1}{\rho_c} (\nabla p_t - \mathbf{q}_d) \right)_{down} = -\mathbf{n} \cdot \mathbf{u}_{tt}$$

$$\mathbf{F}_A = p_{t,down} \mathbf{n} - p_{t,up} \mathbf{n}$$

3.1.6. Mesh 1

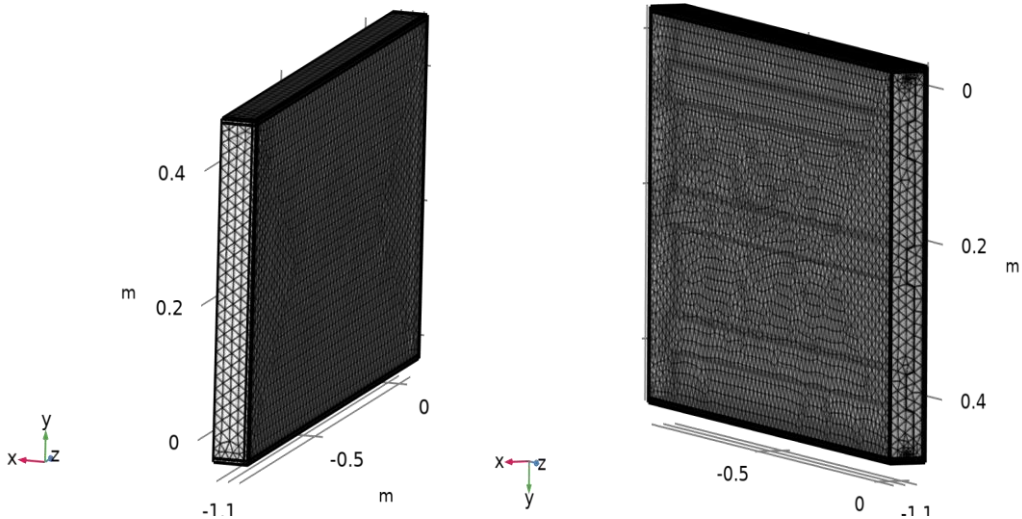


Figure 3.10 Mesh views

3.1.7. Study 1

(This part same for both analyses.)

Frequency Domain

| Frequencies (Hz) | |
|--|--|
| {10, 12.5, 16, 20, 25, 31.5, 40, 50, 63, 80, 100, 125, 160, 200, 250, 315, 400, 500, 630, 800, 1e3, 1.25e3, 1.6e3, 2e3, 2.5e3, 3.15e3, 4e3, 5e3} | |

Study settings

| Description | Value |
|--------------------------------|-------|
| Include geometric nonlinearity | Off |

Settings

| Description | Value |
|-------------|-------|
| Frequencies | |

Physics and variables selection

| Physics interface | Solve for | Equation form |
|---|-----------|------------------------------|
| Pressure Acoustics, Frequency Domain (acpr) | On | Automatic (Frequency domain) |
| Solid Mechanics (solid) | On | Automatic (Frequency domain) |

Physics and variables selection

| Multiphysics couplings | Solve for | Equation form |
|--------------------------------------|-----------|------------------------------|
| Acoustic-Structure Boundary 1 (asb1) | On | Automatic (Frequency domain) |

Store in output

| Interface | Output | Selection |
|---|--------------------|-----------|
| Pressure Acoustics, Frequency Domain (acpr) | Physics controlled | |
| Solid Mechanics (solid) | Physics controlled | |

| Interface | Output | Selection |
|--------------------------------------|--------|-----------|
| Acoustic-Structure Boundary 1 (asb1) | | |

Mesh selection

| Component | Mesh |
|-------------|--------|
| Component 1 | Mesh 1 |

3.1.8. Results

| Description | Value |
|-------------|--|
| Function | Experimental data (int2) |
| Refresh | |

Parameter bounds

| Description | Value |
|-------------|---------|
| Name | t |
| Minimum | -385.53 |
| Maximum | 5428.7 |

Grid

| Description | Value |
|--------------------|---------------------------|
| Resolution | 10000 |
| Point distribution | Mixed uniform/exponential |

Point data

| Description | Value |
|--------------|---|
| Entry method | Coordinates |
| x | 98.99567076891532 123.96310081122705 155.22749877219528 199.29562806489145 244.4161548612513 309.90780126638913 388.0688085870738 496.16835088241334 621.3054295976062 781.2502482509162 982.3702181186761 1250.7966747437056 1553.2638207774219 1945.0082827452648 2445.7185328783753 3113.9956727737135 3915.6424143635363 4944.210726829304 |

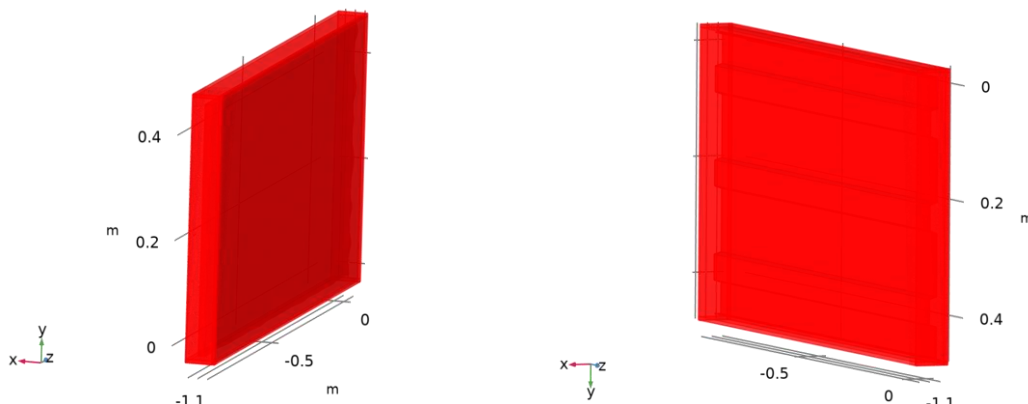


Figure 3.11 Calculation data points and locations view

3.1.9. Datasets

Dataset: Study 1/Solution 1

Tables

Octave Plot Table

Octave band

Table 3-3 Octave band results

| fc (Hz) | Nominal frequency (Hz) | Value Droplet | fc (Hz) | Nominal frequency (Hz) | Value Trapez |
|----------------|-------------------------------|----------------------|----------------|-------------------------------|---------------------|
| 12.589 | 12.5 | 102.25 | 12.589 | 12.5 | 63.314 |
| 15.849 | 16 | 99.29 | 15.849 | 16 | 59.767 |
| 19.953 | 20 | 91.282 | 19.953 | 20 | 50.74 |
| 25.119 | 25 | 86.979 | 25.119 | 25 | 40.152 |
| 31.623 | 31.5 | 86.882 | 31.623 | 31.5 | 38.953 |
| 39.811 | 40 | 81.927 | 39.811 | 40 | 33.491 |
| 50.119 | 50 | 78.568 | 50.119 | 50 | 29.032 |
| 63.096 | 63 | 76.674 | 63.096 | 63 | 26.231 |
| 79.433 | 80 | 71.607 | 79.433 | 80 | 19.538 |
| 100 | 100 | 72.418 | 100 | 100 | 14.575 |
| 125.89 | 125 | 64.574 | 125.89 | 125 | 11.22 |
| 158.49 | 160 | 59.894 | 158.49 | 160 | 17.415 |
| 199.53 | 200 | 52.612 | 199.53 | 200 | 13.09 |
| 251.19 | 250 | 44.834 | 251.19 | 250 | 15.483 |
| 316.23 | 315 | 36.562 | 316.23 | 315 | 16.424 |
| 398.11 | 400 | 17.775 | 398.11 | 400 | 14.004 |
| 501.19 | 500 | 31.656 | 501.19 | 500 | 14.848 |
| 630.96 | 630 | 39.396 | 630.96 | 630 | 17.313 |
| 794.33 | 800 | 39.03 | 794.33 | 800 | 17.37 |
| 1000 | 1000 | 35.981 | 1000 | 1000 | 17.705 |
| 1258.9 | 1250 | 37.662 | 1258.9 | 1250 | 18.284 |
| 1584.9 | 1600 | 44.837 | 1584.9 | 1600 | 19.656 |
| 1995.3 | 2000 | 54.004 | 1995.3 | 2000 | 18.834 |
| 2511.9 | 2500 | 61.559 | 2511.9 | 2500 | 23.713 |
| 3162.3 | 3150 | 67.25 | 3162.3 | 3150 | 22.166 |
| 3981.1 | 4000 | 74.318 | | | |

3.1.10. Plot Groups for droplet

Plot Groups

Indicated Power (three methods)

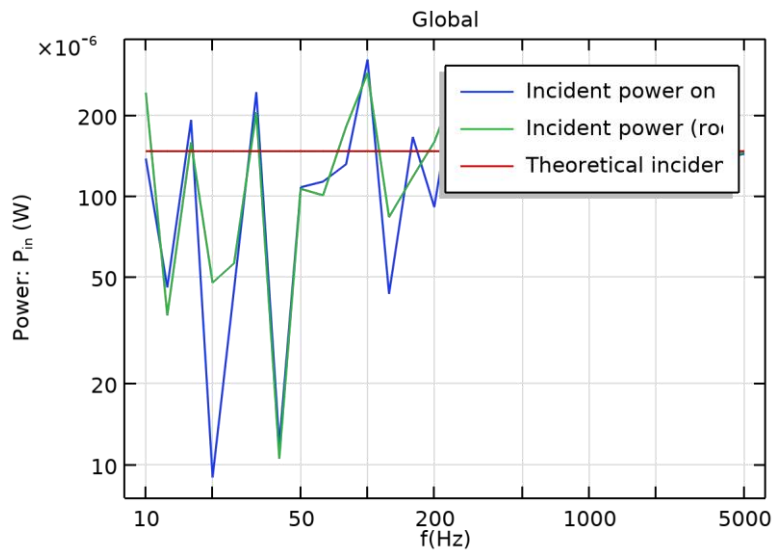


Figure 3.12 Indicated Power graph

Global STL: P_{in}/P_{tr} (1/3 octaves)

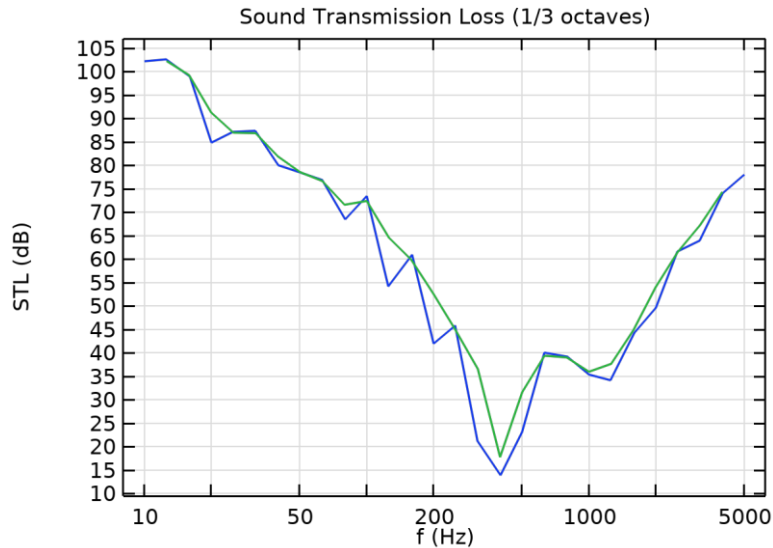


Figure 3.13 STL Sound Transmission Loss Graph

freq(20)=800 Hz Surface: Total acoustic pressure (Pa)

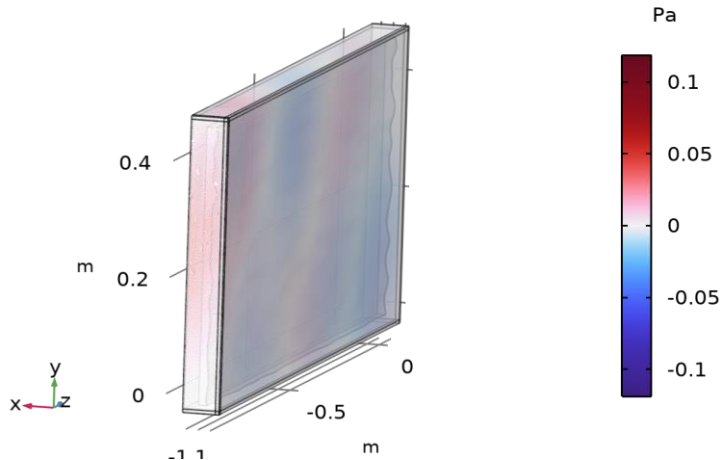


Figure 3.14 Acoustic Pressure (acpr)

Surface: Total acoustic pressure (Pa)

freq(27)=4000 Hz Surface: Total sound pressure level (dB)

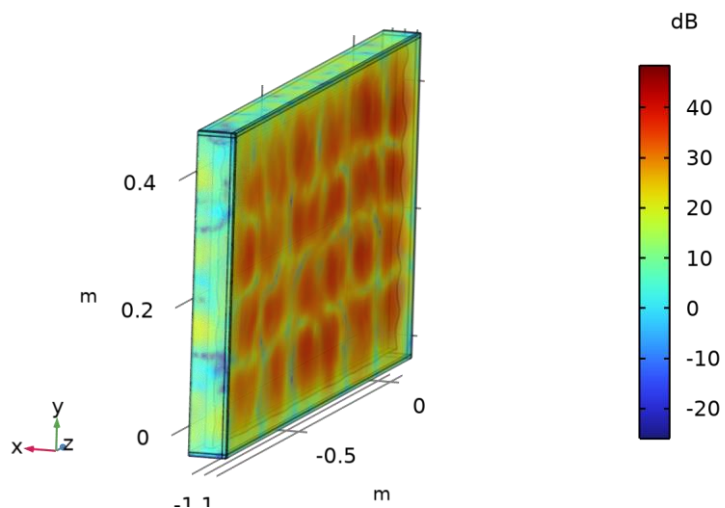


Figure 3.15 Sound Pressure Level (acpr)

Surface: Total sound pressure level (dB)

freq(27)=4000 Hz Isosurface: Total acoustic pressure (Pa)

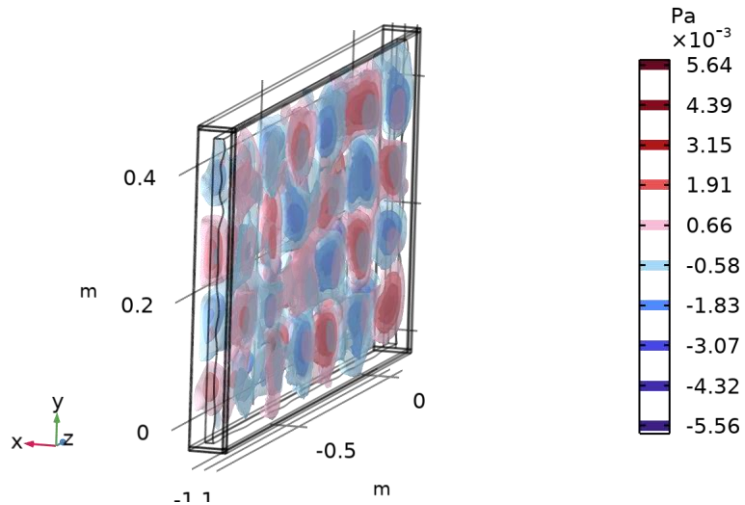


Figure 3.16 Acoustic Pressure, Isosurfaces (acpr)

Isosurface: Total acoustic pressure (Pa)

freq(22)=1250 Hz Volume: Von Mises stress, peak (Pa)

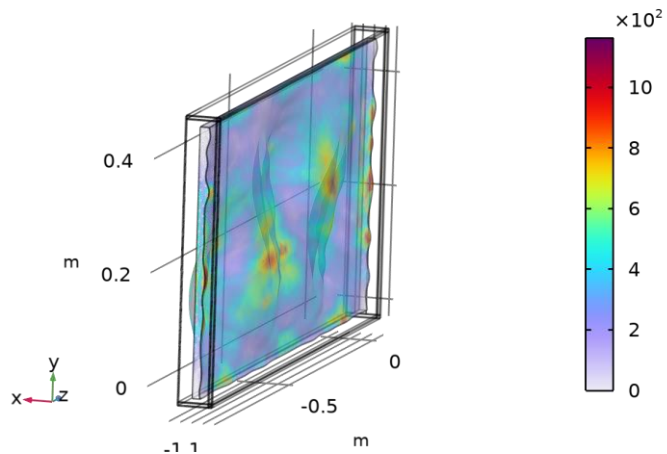


Figure 3.17 Stress (solid)

Volume: Von Mises stress, peak (Pa)

3.1.11. Plot Groups for trapez

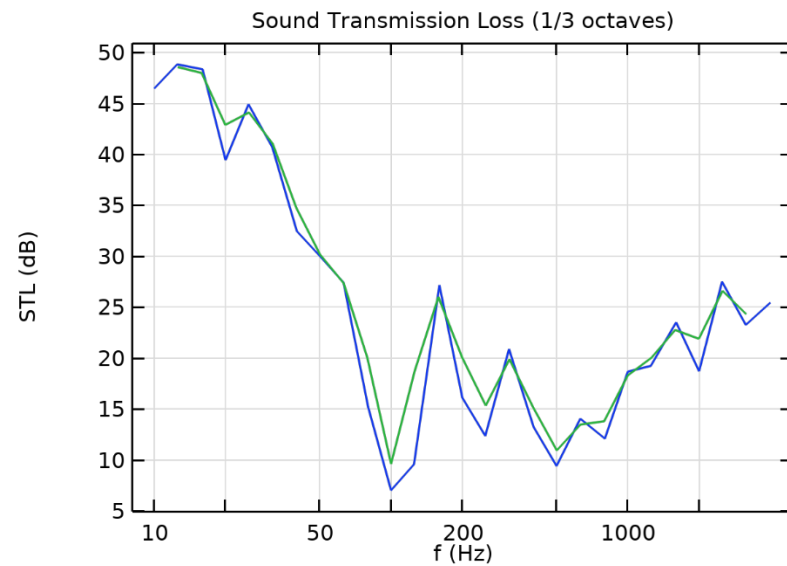


Figure 3.18 STL: P_{in}/P_{tr} (1/3 octaves)

Sound Transmission Loss (1/3 octaves)

`freq(5)=25 Hz Surface: Total acoustic pressure (Pa)`

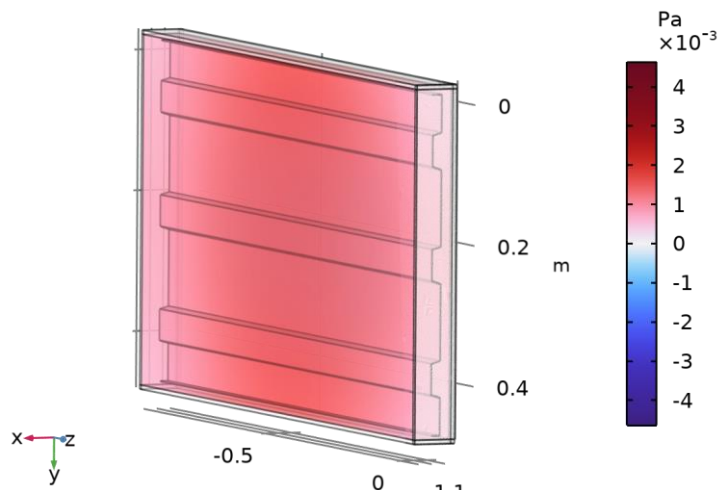


Figure 3.19 Acoustic Pressure (acpr)

Surface: Total acoustic pressure (Pa)

freq(8)=50 Hz Surface: Total sound pressure level (dB)

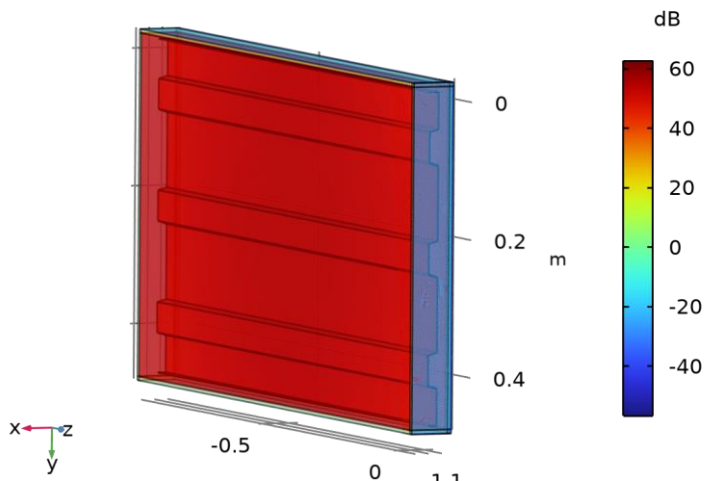


Figure 3.20 Sound Pressure Level (acpr)

Surface: Total sound pressure level (dB)

freq(1)=10 Hz Isosurface: Total acoustic pressure (Pa)

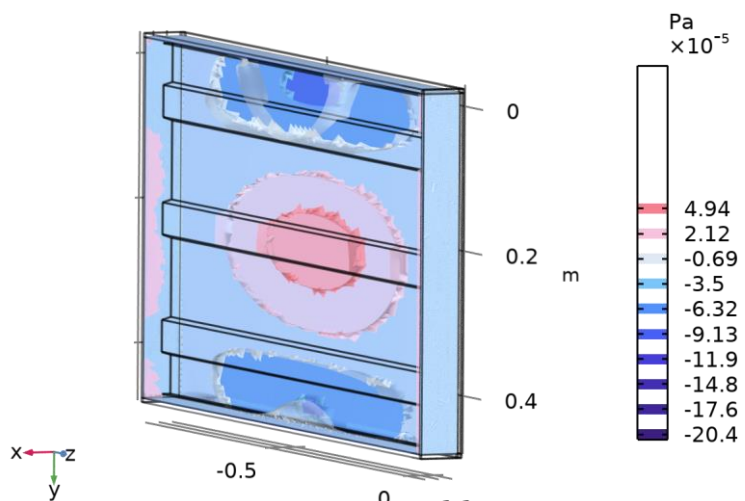


Figure 3.21 Acoustic Pressure, Isosurfaces (acpr)

Isosurface: Total acoustic pressure (Pa)

freq(23)=1600 Hz Volume: Von Mises stress, peak (Pa)

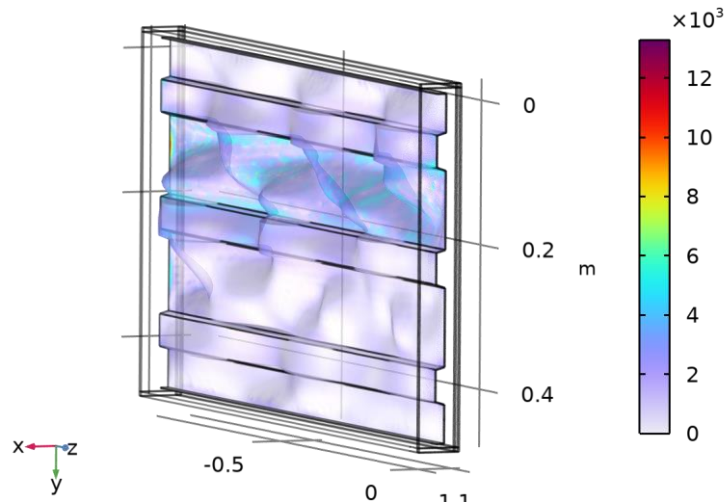


Figure 3.22 Stress (solid)

Volume: Von Mises stress, peak (Pa)

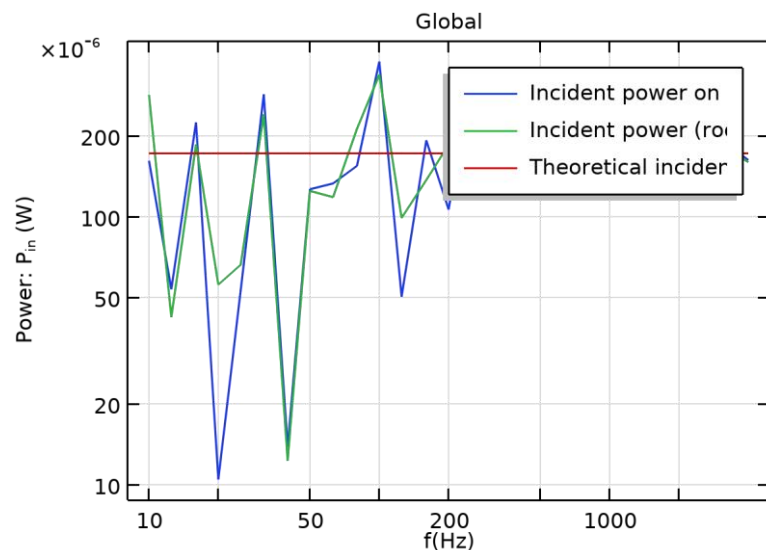


Figure 3.23 Indicated Power (three methods)

4. RESULTS AND COMPARING

Through a comparative analysis utilizing COMSOL Multiphysics software, we've gained valuable insights into the performance of trapezoidal and droplet (waterdrop) models in sound transmission loss (STL) and sound propagation mitigation. Simulations carried out across a wide frequency range in randomized noise environments provided comprehensive data for both models.

Our analysis consistently demonstrated that the water drop design surpasses the trapezoidal model in sound transmission loss across various frequency bands. Validating our findings against test results from Kasso Mühendislik San. ve Tic. A.Ş. for the trapezoidal model, we established a baseline for comparison. Similar analyses were then conducted for the water drop design, aiming for realistic mirroring.

As depicted in Figure 32, our investigation underscores the water drop design's superiority in sound transmission loss, indicating its effectiveness in sound insulation. This finding was further reinforced through validation against certified test results from TSE, ensuring the accuracy and reliability of our computational predictions. Iterative refinement of simulation parameters enhanced the credibility of our study outcomes.

By utilizing MATLAB software, we generated Figure 32, which compares the analysis results of the water drop and trapezoidal designs with the actual experimental results of the trapezoidal design. The graph clearly shows that the experimental and analysis data are closely aligned, substantiating the computational model's precision. This close correlation indicates that the superior performance of the water drop design observed in the analysis is likely to be replicated in real-world applications. Given this alignment, it can be confidently stated that the superior performance of the water drop design observed in the simulations is indicative of its likely superior performance in real-world conditions as well.

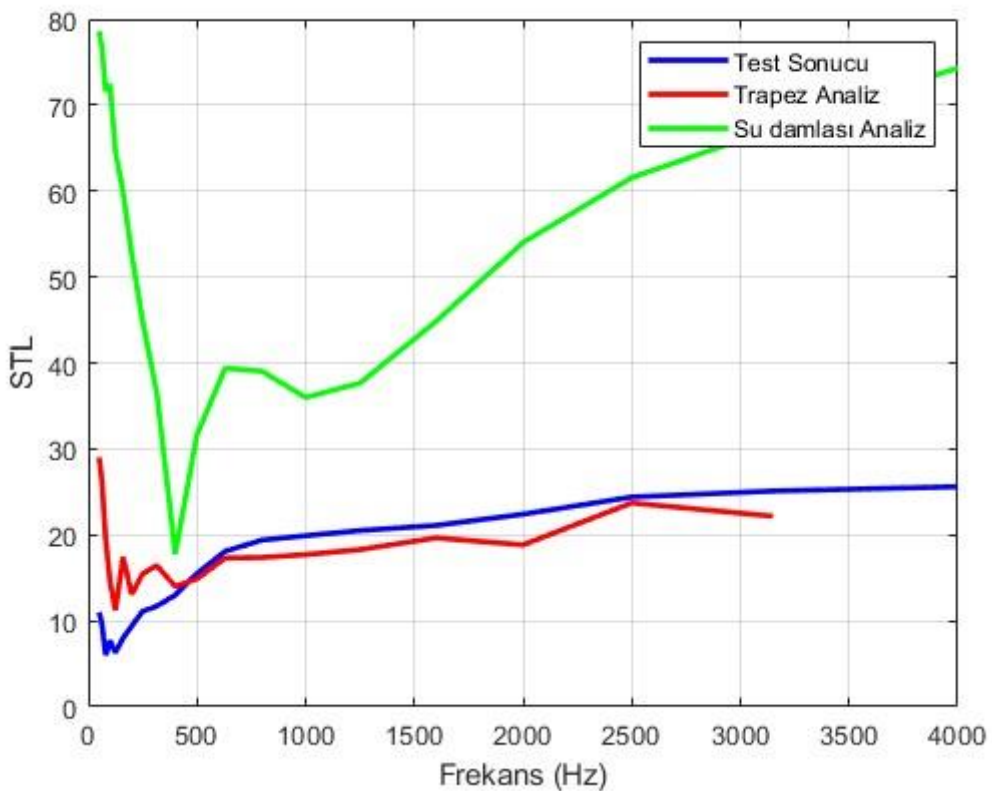


Figure 4.1 Comparison of analysis results of water drop and trapezoidal design with actual experimental results of trapezoidal design.

This study demonstrates that the same methodology can be employed to evaluate any desired design. By using advanced simulation tools like COMSOL Multiphysics and MATLAB for data analysis, we can reliably predict the performance of various sound insulation designs, thereby facilitating informed decisions in the development of new noise barrier systems. The versatility of this approach means it can be adapted to assess different geometric configurations and materials, making it a robust tool for sound insulation research.

4.1. LIMITATIONS AND CONSIDERATIONS

It's important to note that due to the lack of sufficiently competent software for comprehensive sound barrier analysis, our study focused on evaluating the surface geometry of the designs rather than the entire structure. We assumed the same absorbing materials between surfaces to reduce computational load and focus on the variable dependent on surface geometry. This approach allowed us to isolate and analyse the impact of design geometry on sound insulation performance without the added complexity of varying material properties.

Specifically, the analysis was limited to the surface geometry because current software

solutions do not fully support comprehensive simulations of complete sound barrier systems. By maintaining consistent absorbing materials between surfaces, we simplified the analysis, allowing for a focused examination of geometric influences on sound insulation. This methodological choice helped to manage computational intensity and streamline the evaluation process.

While the water drop design excels in sound insulation, we must acknowledge the merits of the trapezoidal model. Despite its comparative disadvantage in sound transmission loss, the trapezoidal model remains relevant due to factors such as ease of production and cost-effectiveness. Nevertheless, the water drop design not only outperforms in sound insulation but also boasts aesthetic superiority, offering a visually striking appearance that elevates architectural and urban design.

Embracing innovative designs like the water drop model can enhance both functionality and visual appeal in architectural solutions. This research underscores the need for a holistic approach that balances functional and aesthetic considerations in the development of sound-insulating materials and systems.

In conclusion, this study sheds light on sound insulation technology and emphasizes the importance of aesthetics in design decisions. The water drop design's superior performance in mitigating sound propagation, combined with its visual sophistication, makes it a valuable solution for enhancing urban living standards. By embracing innovative designs like the water drop model, industries can achieve a balance between functionality and visual harmony, ultimately enhancing urban environments.

4.2. OVERALL COMPARISON

The comparative analysis favours the water drop design over the trapezoidal model in both sound insulation effectiveness and aesthetic appeal. While the trapezoidal model has practical advantages, such as ease of production, the water drop design offers superior performance in mitigating sound propagation and adds visual sophistication to architectural and urban design. Balancing functionality and aesthetics is crucial in developing sound-insulating materials and systems to enhance urban living standards.

4.3. EVALUATION OF CURRENT WORK FROM MUDEK PERSPECTIVE

4.3.1. Economic Analysis

From an economic standpoint, both designs present distinct cost implications across the production, installation, and maintenance phases. The trapezoidal design is economically advantageous due to its simpler geometry, which requires less material and involves straightforward manufacturing processes. This simplicity translates to lower production costs and faster manufacturing times, making it a cost-effective option for large-scale

implementation. On the other hand, the water drop design, with its intricate and aesthetically pleasing structure, incurs higher initial costs due to the complexity of its production. Advanced manufacturing techniques and more materials are necessary, driving up expenses. However, the superior sound insulation performance of the water drop design offers long-term economic benefits by potentially increasing property values and reducing healthcare costs associated with noise pollution. Additionally, its visual appeal can enhance the marketability of properties and public spaces, providing an economic boost through increased desirability.

4.3.2. Real-Life Conditions

In real-life conditions, the performance, durability, and maintenance requirements of the designs come to the fore. The water drop design excels in mitigating sound propagation, as evidenced by comparative analyses and simulations, making it particularly effective in urban environments with high noise levels. However, its complex shape might lead to challenges in terms of debris accumulation and cleaning, requiring more frequent and detailed maintenance. The trapezoidal design, though less effective in sound insulation, benefits from easier maintenance due to its simpler shape. Both designs must endure environmental stresses such as weather conditions, but the robust metallic construction of both ensures durability. Detailed field tests are essential to validate their long-term performance under varying environmental conditions.

4.3.3. Producibility

Producibility is a crucial factor in determining the feasibility of these designs for widespread adoption. The trapezoidal model, with its straightforward geometry, can be efficiently produced using standard manufacturing processes, ensuring scalability and cost-efficiency. This makes it an ideal choice for projects with tight budgets and urgent timelines. Conversely, the water drop design requires more sophisticated manufacturing techniques, such as CNC machining or advanced forming, which increases production time and costs. While these advanced techniques can be more challenging, they also open up possibilities for innovative manufacturing approaches like 3D printing, which could eventually make the water drop design more accessible for mass production.

4.3.4. Constraints

Various constraints, including regulatory, spatial, and technical limitations, impact the implementation of these designs. Regulatory compliance is mandatory for both designs to meet local and international standards for noise barriers, affecting material choice and design specifications. Spatial constraints are particularly relevant for the water drop design, which may require more installation space due to its complex shape, limiting its application in densely populated urban areas. Technically, the trapezoidal design's simplicity allows for easier integration with existing infrastructure, while the water drop design may necessitate custom solutions, increasing complexity and cost. Additionally, both designs must address

material sustainability to minimize environmental impact, prioritizing eco-friendly materials and energy-efficient manufacturing processes. Current software limitations in comprehensive sound barrier analysis also influenced our study, focusing primarily on surface geometry to manage computational load while assuming consistent absorbing materials between surfaces.

In conclusion, the water drop design offers superior sound insulation and aesthetic benefits but comes with higher initial costs and maintenance challenges. The trapezoidal design, while less effective in noise reduction, is more practical, cost-effective, and easier to produce and maintain. Balancing these factors is essential to selecting the most appropriate design for specific urban environments, ensuring that functionality, aesthetics, and economic viability are harmonized to enhance urban living standards.

5. CONCLUSION

This study has demonstrated the superiority of the water drop design over the trapezoidal model in both sound insulation effectiveness and aesthetic appeal. While the trapezoidal model offers practical advantages such as ease of production, the water drop design excels in mitigating sound propagation and adds visual sophistication to architectural and urban design.

The comparative analysis using COMSOL Multiphysics software, conducted over a wide frequency range in random noise environments, revealed that the water drop design consistently outperforms the trapezoidal model in terms of sound transmission loss (STL) across various frequency bands. These findings were confirmed through simulations and verified test results, highlighting the water drop design's potential to enhance urban living standards by improving the quality of life in urban environments.

Furthermore, the study emphasizes the importance of balancing functionality and aesthetics in the development of sound-insulating materials and systems. The water drop design's ability to effectively mitigate sound propagation and its visually striking appearance make it an attractive solution for architects, urban planners, and policymakers.

The results underscore the need for a holistic approach to urban planning and design that considers the interplay between sound insulation, aesthetics, and functionality. By embracing innovative designs like the water drop model, industries can create more liveable and sustainable urban environments that prioritize the well-being of citizens.

REFERENCES AND AUXILARY RESOURCES

1. Moser, M. (2004). *Engineering Acoustics: An Introduction to Noise Control*. Berlin, Germany: Springer Science.
2. Raichel, D. R. (2006). *The Science and Applications of Acoustics* (2nd ed.). New York, USA: Springer Science.
3. Degischer, H.-P., & Kriszt, B. (Eds.). (2002). *Handbook of Cellular Materials: Production, Processing, Applications*. Weinheim, Germany: WILEY-VCH.
4. Rossing, T. D. (Ed.). (2007). *Springer Handbook of Acoustics*. New York, USA: Springer Science.
5. Le, C. H. (2010). *Developments in topology and shape optimization*. Ph.D. Thesis, University of Illinois at Urbana-Champaign.
6. Eschenauer, H. (Ed.). (2006). *IUTAM Symposium on Topological Design Optimization of Structures, Machines and Materials*. Dordrecht, Netherlands: Springer.
7. Joshi, H. R. (2013). *Finite Element Analysis of Effective Mechanical Properties, Vibration, and Acoustic Performance of Auxetic Chiral Core Sandwich Structures*. M.Sc. Thesis, Purdue University.
8. Ramnath, B. V., Alagarraja, K., & Elanchezhian, C. (2019). Influence of fiber orientation on the mechanical properties of GFRP composites. *Materials Today: Proceedings*, 16, 859-864.
9. Sayahlatifi, S., Rahimi, G., & Bokaei, A. (2021). An investigation into the acoustic performance of sandwich structures with auxetic cores. *Journal of Sandwich Structures and Materials*, 23, 94-109.
10. Li, Y., Wang, F., Jia, S., Ma, X., & Zhang, Y. (2021). Influence of process parameters on the mechanical properties of fiber-reinforced polymers. *Fibers and Polymers*, 22, 1718-1726.
11. Florence, M., Jaswin, M. A., & Pandi, A. P. (2020). Investigation of the tensile properties of fiber-reinforced polymers. *Fibers and Polymers*, 21, 1152-1160.
12. Arunkumar, M. P., Pitchaimani, J., Gangadharan, K. V., & Babu, M. C. L. (2017). Dynamic analysis of sandwich structures with auxetic core. *Journal of Sandwich Structures and Materials*, 19, 26-42.
13. Griesse, D., Summers, J. D., & Thompson, L. (2015). Structural health monitoring of sandwich composites using vibration analysis. *Journal of Vibration and Acoustics*, 137, 021011.
14. Reiter, P., Wehr, R., & Ziegelwanger, H. (2017). Simulation and measurement of noise barrier sound-reflection properties. *Applied Acoustics*, 121, 11-21.

15. Moore, J. A., & Lyon, R. H. (1991). Sound transmission loss characteristics of sandwich panel constructions. *Journal of the Acoustical Society of America*, 89(3), 1544-1552.
16. Halliwell, R. E., & Warnock, A. C. C. (1985). Sound transmission loss: Comparison of conventional techniques with sound intensity techniques. *The Journal of the Acoustical Society of America*, 77(6), 2094-2103.
17. Garai, M., & Guidorzi, P. (2015). Sound reflection measurements on noise barriers in critical conditions. *Applied Acoustics*, 98, 103-109.
18. Xiong, W. 2010. *Applications of COMSOL Multiphysics Software to Heat Transfer Processes*
19. Song, Y., Wen, J., Tian, H., Lu, X., Li, Z., & Feng, L. (2020). Vibration and sound properties of metamaterial sandwich panels with periodically attached resonators: Simulation and experiment study. *Journal of Sound and Vibration*, 486, 115559
20. Khrystoslavenko, O., & Grubliauskas, R. (2017). Simulation of room acoustics using COMSOL Multiphysics. In *Proceedings of the 20th Conference for Junior Researchers "Science – Future of Lithuania" Environmental Protection Engineering* (Article No. aplinka.06). Vilnius, Lithuania: Vilnius Gediminas Technical University
21. Saadeghvaziri, M. A., & Macbain, K. (1998). Sound barrier applications of recycled plastics. *Transportation Research Record: Journal of the Transportation Research Board*, 1626(1), 83-89.
22. Bolton, J. S., Shiau, N.-M., & Kang, Y. J. (1995). Sound transmission through multi-panel structures lined with elastic porous materials. *Journal of Sound and Vibration*, 191(3), 317-347.
23. Oh, Y. K., & Kim, H. G. (2023). A preliminary study on the measurement method for determining the absorption coefficient of sound barrier panels [방음판의 흡음률 측정방법 제안을 위한 기초 연구]. *The Journal of the Acoustical Society of Korea*, 42(2), 152-160.
24. Oh, Y. K. (2022). A study on the standard for determining airborne sound insulation performance of sound barrier panels [방음판의 음향투과손실 측정규격에 관한 연구]. *Journal of Architectural Acoustics*, 35(3), 123-135.
25. Asdrubali, F., & Pispoli, G. (2007). Properties of transparent sound-absorbing panels for use in noise barriers. *Journal of Sound and Vibration*, 302(4-5), 840-854.
26. Schiller, N. H., Jones, M. G., & Bertolucci, B. (2017). Experimental evaluation of acoustic engine liner models developed with COMSOL Multiphysics. *Journal of Sound and Vibration*, 398, 311-326.

27. Khrystoslavenko, O., & Grubliauskas, R. (2017). Simulation of room acoustics using COMSOL Multiphysics. *Proceedings of the 20th Conference for Junior Researchers*
28. Ekici, I., & Bougdah, H. (2003). A review of research on environmental noise barriers. *Journal of Environmental Engineering*, 129(12), 1065-1073
29. May, D. N., & Osman, N. M. (1980). Highway noise barriers: New shapes. *Journal of Sound and Vibration*, 71(1), 73-101
30. Ishizuka, T., & Fujiwara, K. (2004). Performance of noise barriers with various edge shapes and acoustical conditions. *Applied Acoustics*, 65(2), 125-141.
31. Laxmi, V., Thakre, C., & Vijay, R. (2022). Evaluation of noise barriers based on geometries and materials: A review. *Environmental Science and Pollution Research*, 29(10), 1729-1745.
32. Kotzen, B., & English, C. (2009). *Environmental noise barriers: A guide to their acoustic and visual design* (2nd ed.). London: CRC Press.

Auxilary Web Sites: [Last access date: 30.05.2024]

- <https://www.comsol.com/model/sound-transmission-loss-through-a-concrete-wall-73371>
- <https://www.comsol.com/model/sound-transmission-loss-through-a-window-85201>
- <https://www.astm.org/e0090-09r16.html>
- <https://www.schuette-aluminium.de/en/professional-noise-protection/noise-barriers-acoustic-barriers>
- <https://www.astm.org/e1332-22.html>
- <https://www.journals.elsevier.com/applied-acoustics>
- <https://www.icacommission.org/>
- <https://acousticstoday.org/>
- <https://www.fhwa.dot.gov/>
- <https://www.soundflow.afmng.eu>
- <https://doi.org/10.3846/aainz.2017.06>
- <https://www.acoustic-barriers.com/>
- https://ec.europa.eu/environment/noise/roads/noise_barriers_en.htm

APPENDICES

A1: #Matlab code for plotting Figure 32#

```
% Test Sonucu
frekans = [50, 63, 80, 100, 125, 160, 200, 250, 315, 400, 500, 630, 800, 1000,
1250, 1600, 2000, 2500, 3150, 4000];
R_1_3_oktav = [11.0, 9.6, 6.0, 7.7, 6.3, 8.0, 9.4, 11.1, 11.7, 13.0, 15.5,
18.1, 19.4, 19.9, 20.5, 21.1, 22.4, 24.4, 25.1, 25.6];

% Trapez Analiz
frekans2 = [50, 63, 80, 100, 125, 160, 200, 250, 315, 400, 500, 630, 800, 1000,
1250, 1600, 2000, 2500, 3150];
value2 = [29.032, 26.231, 19.538, 14.575, 11.22, 17.415, 13.09, 15.483, 16.424,
14.004, 14.848, 17.313, 17.37, 17.705, 18.284, 19.656, 18.834, 23.713, 22.166];

% Su daması Analiz
frekans3 = [50, 63, 80, 100, 125, 160, 200, 250, 315, 400, 500, 630, 800, 1000,
1250, 1600, 2000, 2500, 3150, 4000];
value3 = [78.568, 76.674, 71.607, 72.418, 64.574, 59.894, 52.612, 44.834,
36.562, 17.775, 31.656, 39.396, 39.03, 35.981, 37.662, 44.837, 54.004, 61.559,
67.25, 74.318];

% Çizgi grafiğini oluştur
plot(frekans, R_1_3_oktav, 'b', 'LineWidth', 2);
hold on;
plot(frekans2, value2, 'r', 'LineWidth', 2);
plot(frekans3, value3, 'g', 'LineWidth', 2);
xlabel('Frekans (Hz)');
ylabel('STL');
grid on;

% Şekil açıklamalarını ekle
legend('Test Sonucu', 'Trapez Analiz', 'Su daması Analiz');
```

| | | | | |
|--|---|---|--|---|
|  <p>TÜRK STANDARDLARI ENSTİTÜSÜ DENEY ve KALİBRASYON MERKEZİ BAŞKANLIĞI YAPI MALZEMELERİ YANGIN VE AKUSTİK LABORATUVAR MÜDÜRLÜĞÜ</p> <p>TURKISH STANDARDS INSTITUTION HEADSHIP OF TSE TEST and CALIBRATION CENTER CONSTRUCTION MATERIALS FIRE AND ACOUSTICS LABORATORY</p> <p>AYDINLI MAH. ULUS SOK. NO:7/1 TUZLA/İSTANBUL</p> <p>Tel: +902165600561 Faks: e-mail: yalitim@tse.org.tr www.tse.org.tr</p> |  <p>ILAC-MRA</p>  <p>TÜRKAK Test TS EN ISO/IEC 17025 AB-0001-T</p> <table border="1" style="margin-left: auto; margin-right: auto;"> <tr><td>AB-0001-T</td></tr> <tr><td>9437</td></tr> <tr><td>03-22</td></tr> </table> | AB-0001-T | 9437 | 03-22 |
| AB-0001-T | | | | |
| 9437 | | | | |
| 03-22 | | | | |
| MUAYENE VE DENEY RAPORU TEST REPORT | | | | |
| <p>Deneyi Talep Eden/Firma : <i>(Adı, Adresi, Şehir vb.)</i> Requesting/Customer <i>(Name, Address, City etc.)</i></p> <p>Deney Talep Tarih / No : <i>Order Date/No.</i> 6.01.2022 / 2022-3193</p> <p>Numunenin Tanımı : <i>(Cins, Marka, Simf, Tip, Tür, Model vb.)</i> Sample Description (Type,Mark,Class,Model etc.) 2022-001328 , SES BARIYERİ , - , - , - , - , AKUSTİK BARIYER , 1.00 adet</p> <p>Numune Kabul Tarihi : <i>Test Item Receipt Date</i> 24.02.2022</p> <p>Deneylerin Yapıldığı Tarih : <i>Date of Test</i> 24.02.2022 / 09.03.2022</p> <p>Uygulanan Standart Metot : <i>Applied Standard/Method</i> , TS EN 1793-2/-, TS EN 1793-3:2002/-</p> <p>Raporun Sayfa Sayısı : <i>Number of pages of the report</i> 11</p> <p>Deney Sonucu : <i>Results</i> -</p> <p>Açıklamalar : <i>Remarks</i></p> | | | | |
| <p>Yukarıda tanımlanan numune için laboratuvarımızda yapılan muayene ve deneylerden elde edilen sonuçlar müteakip sayfalar da verilmiştir. <i>The testing and/or measurement results are given on the following pages which are part of this report.</i></p> <p>Deney laboratuvarları olarak faaliyet gösteren TSE Deney ve Kalibrasyon Merkezi Başkanlığı Deney Laboratuvarları TÜRKAK'tan AB-0001-T ile TS EN ISO/IEC 17025:2012 standartına göre akredite edilmiştir. <i>TSE Headship of Test and Calibration Center Testing Laboratories accredited by TÜRKAK under registration number AB-0001-T for TS EN ISO/IEC 17025:2017 as test laboratory.</i></p> <p>TÜRKAK deney raporlarının tanınımı konusunda Avrupa Akreditasyon Birliği (EA) ile Çok Taraflı Anlaşma ve Uluslararası Laboratuvar Akreditasyon Birliği(ILAC) ile karşılıklı tanınma anlaşması imzalamıştır. <i>TÜRKAK is a signatory to the European co-operation for Accreditation (EA) Multilateral Agreement (MLA) and to the International Laboratory Accreditation Cooperation (ILAC) Mutual Recognition Arrangement (MRA) for the recognition of test reports.</i></p> <p>Deneyle veya ölçüm sonuçları, genetleştirilmiş ölçüm belirsizlikleri (olması halinde) ve deney metodları bu raporun tamamlayıci kismı olan takip eden sayfalarda verilmiştir. <i>The test and/or measurement results, the uncertainties (if applicable) with confidence probability and test methods are given on the following pages which are part of this report.</i></p> | | | | |
| Mühür <i>Seal</i>  | Tarih <i>Date</i> 09.03.2022 | Deneys Sorumlusu <i>Person in charge of test</i> MEHMET HÜDAİ BAŞTÜRK | Kontrol Eden <i>Reviewer</i> HALİL ALPER YILDIRIM | Onaylayan <i>Head of Laboratory</i> SENCER GÜVEN |
| <p>Bu rapor, hazırlayan laboratuvarın yazılı izni olmadan kısmen kopyalanıp çoğaltılamaz. İmzasız ve karekodlu raporlar geçersizdir. Bu rapor, sadece deneyi yapılan numune için geçerlidir ve "Ürün Belgesi" yerine geçmez. <i>This test report shall not be reproduced other than in full except with the written permission of the laboratory. Test reports without signature and seal are not valid. This test report represents only tested sample(s), and shall not be used as Product Certificate.</i></p> <p style="text-align: center;">Bu doküman elektronik ortamda imzalanmıştır. Dogrulama adresi: https://basvuru.tse.org.tr/uye/QRKodDogrulama?code=9FCDF4</p> | | | | |

Figure B1: Experimental Test Report Information



TSE DENEY ve KALİBRASYON MERKEZİ BŞKANLIĞI YAPI MALZ. YANGIN VE AKUSTİK LAB.
HEADSHIP OF TSE TEST and CALIBRATION CENTER CONST. MAT. FIRE AND ACOUSTICS LABORATORY

MUAYENE - DENYEY SONUÇLARI TEST RESULTS
TS EN 1793-2:2018 ; TS EN 1793-3:2002

AB-0001-T
9437
03-22

| | |
|--|--|
| Deney Laboratuvarının Adı ve Adresi | TSE Yapı Malz. Yangın ve Akustik Laboratuvarı Akustik Bölümü Aydınlı Mah. Ulus Sokak No:7/1 Tuzla/İSTANBUL |
| Deneyi Talep Eden Kuruluşun Adı ve Adresi | İŞIK PLASTİK SANAYİ VE DIŞ TİCARET PAZARLAMA ANONİM ŞİRKETİ Gebze Organize Sanayi Bölgesi Mustafapaşa Mah. İhsandede Cad.No:101 GEBZE/KOCAELİ/TÜRKİYE |
| Numune Tipi | Ses Bariyeri |

1. Giriş

İŞIK PLASTİK SANAYİ VE DIŞ TİCARET PAZARLAMA ANONİM ŞİRKETİ'nin talebi üzerine “Ses Bariyerinin” hava doğuşlu ses yalıtımı değerinin belirlenmesi amacıyla “TS EN 1793-2:2018 Yollardaki trafik gürültüsünü azaltıcı sistemler – Akustik performansın tayini için deney yöntemi - Bölüm 2: Düzgün dağılmış ses alanı koşullarında hava ile yayılan sesin yalıtımına ait temel özellikler” standardına göre 25.02.2022 tarihinde TSE Yapı Malz. Yangın ve Akustik Laboratuvarında deney yapılmıştır.

2. Deney Odaları

Deney odaları, TS EN ISO 10140-2, TS EN ISO 10140-5 ve TS EN 1793-2 standartlarında belirtilen tüm gerekleri karşılamaktadır. Boyutlar şekil ve yerleşim koşulları raporun sonunda sunulmuştur.

| | |
|-------------------------|---------------------------|
| Kaynak oda hacmi | 114,9m³ |
| Alici oda hacmi | 174,4m³ |
| Deney açılılığı | 12,4m² |

| | | | |
|---------------|-----------------|--------------|---------------|
| Deney odaları | Sıcaklık [°C] | Basınç [kPa] | Bağıl nem [%] |
| Alici oda | 22,4±0,8 | 100,9±1 | 47,0±5 |
| Kaynak oda | 22,1±0,8 | 100,9±1 | 42,4±5 |

3. Deney numunesi

Deney numunesi firma tarafından seçilmiş ve laboratuvarımıza ulaştırılmıştır.
Numunenin üretim tarihi:2022
Numunenin laboratuvara ulaşma tarihi: 02.2022

2/11

LAB-D-FR-36 / 11.06.2020 - 6

Figure B2: Experimental Test Report Room properties



MUAYENE - DENEY SONUÇLARI TEST RESULTS
TS EN 1793-2:2018 ; TS EN 1793-3:2002

3.1 Deney numunesinin tanımlanması

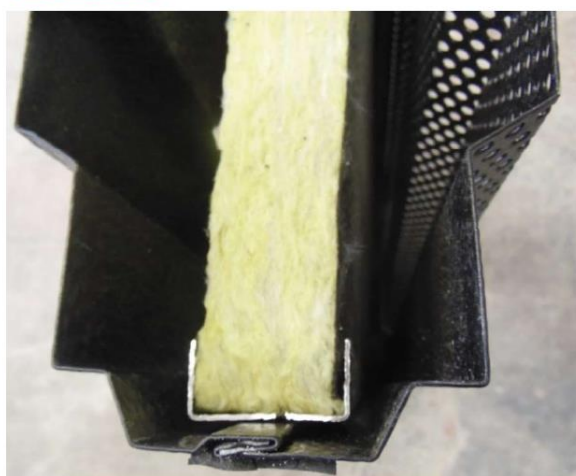
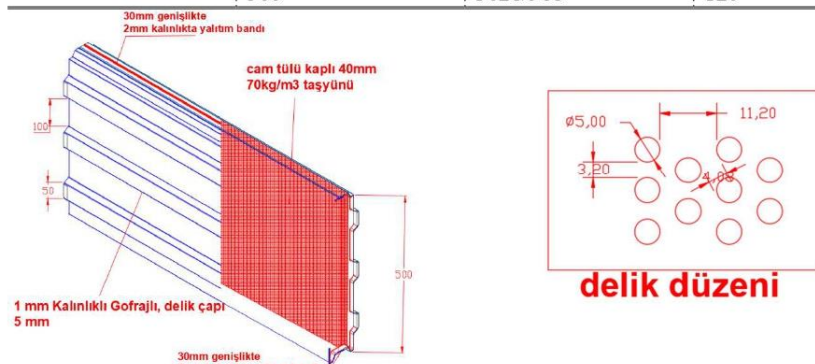
Ürün tanımı: 1 mm kalınlığında gofrajlı alüminyum levhalarla oluşturulmuş 500 mm eninde, muhtelif boylarda, 120 mm kalınlığında, ön yüzü delikli (delik çapı 5mm) ve orta kısımda bir yüzü cam tülü kaplı yaklaşık 40mm kalınlığında 70kg/m³ yoğunlukta taş yünü bulunan ses bariyeri. Numune ortasında HEA 160 dikme kullanılmıştır.

Malzemesi: Delikli/Deliksiz gofrajlı alüminyum levha (boyalı kalınlık ≈1,45mm), cam tülü kaplı taş yünü.

Panel ağırlığı (975*500*120mm): 5,6 kg

Numunenin yüzey alanı: ≈11,9 m²

| Boytular (2 tip) | Genişlik (mm) | Uzunluk (mm) | Kalınlık (mm) |
|------------------|---------------|--------------|---------------|
| | 500 | 3028/968 | 120 |



*Ürün tanımlamalarında firma beyanı kullanılmıştır.

Figure B3: Experimental Test Report test sample panel properties



3.2 Deney numunesinin montajı

*Deney çerçevesi TS EN ISO 10140-5'e uygun olarak seçilmiştir. Deney çerçevesinin boyutları 3,06 m x 4,06 m'dir.

*Deney numunesi bütün olarak laboratuvara getirilmiş ve çerçeveye yerleştirilmiştir.

*Panellerin ön ve arkasında, yan ve üst taraflara L50*50 profil, yerleştirilmiştir. Betonarme çerçeve ile numune arasında hava kaçağı olmaması için yalıtım macunu ve filıl kullanılmıştır.

*Deney numunesinin orta kısmında HEA 160 profilinden mamul dikme kullanılmıştır.

*Deney numunesinin deney çerçevesinin içeresine yerleştirilmesi firma tarafından yapılmıştır.

*Deney çerçevesinin deney odalarının arasına yerleştirme işlemi laboratuvar tarafından yapılmıştır.

4. Yöntem

Deney tesisi **TS EN ISO 10140-5**, **TS EN ISO 10140-2** ve **TS EN 1793-2** standartlarında belirtilen özelliklerin tamamını karşılamaktadır.

- Biri kaynak oda diğeri alıcı oda olacak şekilde yatayda birbirine bitişik olan iki oda kullanılmıştır.
- Deney numunesi çerçeveye “Deney numunesinin montajı” başlıklı **3.2 Maddesinde** belirtildiği şekilde yerleştirilmiştir.
- Hoparlör ve mikrofonlar daha önceden belirlenen ölçüm noktalarında konumlandırılarak sistem ölçüme hazır hale getirilmiştir.
- Ölçüme başlamadan hemen önce mikrofonlarla doğrulama işlemi yapılmıştır.
- Hareketli mikrofonun kullanıldığı ölçümlerde ölçüm süresi **60 sn** ve hareketli mikrofonun bir tam tur dönüş süresi **60 sn** olacak şekilde ses basınç seviyesi ölçümleri yapılmıştır.
- TS EN ISO 3382 standardına göre her frekans bandı için **12 ölçüm** (2 kaynak konumu , 6 mikrofon konumu) yapılarak alıcı odasındaki çınlama süresi bulunmuştur.
- Alıcı odada arka plan gürültüsü ölçülerek ses basınç düzeylerinin hesabında gerekli düzeltmeler yapılmıştır.
- Sonuçlar TS EN ISO 10140-2 ve TS EN ISO 10140-1 standardlarında yer alan aşağıdaki formüle göre hesaplanmıştır.

$$R=L_1-L_2+10\log(S/A)$$

$$A=0,16V/T$$

Burada;

L₁: Kaynak odadaki ses basınç seviyesi enerji ortalaması, desibel

L₂: Alıcı odadaki ses basınç seviyesi enerji ortalaması, desibel

S: Deney elemanın yerleştirileceği serbest deney açığlığının alanı, m²

A: Alıcı odadaki eşdeğer ses absorpsiyon alanı, m²

V: Alıcı odanın hacmi, m³

4/11

LAB-D-FR-36 / 11.06.2020 - 6

Figure B4: Experimental Test Report Standart and Method



TSE DENEY ve KALİBRASYON MERKEZİ BŞKANLIĞI YAPI MALZ. YANGIN VE AKUSTİK LAB.
HEADSHIP OF TSE TEST and CALIBRATION CENTER CONST. MAT. FIRE AND ACOUSTICS LABORATORY

MUAYENE - DENEY SONUÇLARI TEST RESULTS
TS EN 1793-2:2018 ; TS EN 1793-3:2002

| |
|-----------|
| AB-0001-T |
| 9437 |
| 03-22 |

T: Alıcı odada çınlama süresi, s

- TS EN 1793-3 standardında verilen normalize trafik spektrumu değerleri kullanılarak DL_R , aşağıda verilen denkleme göre desibel cinsinden hesaplanmıştır.

$$DL_R = -10 \lg \left| \frac{\sum_{i=1}^{18} 10^{0.1L_i} 10^{-0.1R_i}}{\sum_{i=1}^{18} 10^{0.1L_i}} \right|$$

Burada;

DL_R Hava ile yayılan ses yalıtımına ait performansın, A-ağırlıklı ses basınç seviyelerinin bir farkı olarak desibel cinsinden ifade edilen tek sayı derecelendirmesidir.

R_i .i'inci 1/3 oktav banttaki ses azaltım indeksidir.

L_i EN 1793-3'de tanımlanan i'inci 1/3 oktav banttaki trafik gürültüsünün normalize edilmiş A-ağırlıklı, desibel cinsinden ses basınç seviyesidir.

- Hava ile yayılan ses yalıtım performans sınıflandırılması TS EN 1793-2 standardının Ek A'sına uygun olarak yapılmıştır.

5. Gözlemler

*Paneller arasında, birleşim yerlerinde yalıtım bandı (30mm genişlik-2mm kalınlık) kullanılmıştır.

*Çerçeve ile numune birleşim yerlerinde L profiller kullanılmıştır.

*Numunenin en alt kısmında epdm filit kullanılmıştır.

6. Sonuç

Ses azaltma indekslerinin 1/3 oktav bantlardaki değerleri tablo ve grafik olarak aşağıda verilmiştir.

TS EN 1793-2 standardına göre ses azaltım indeksinin tek sayı değeri **$DL_R 16 dB$** olarak bulunmuştur.

5/11

LAB-D-FR-36 / 11.06.2020 - 6

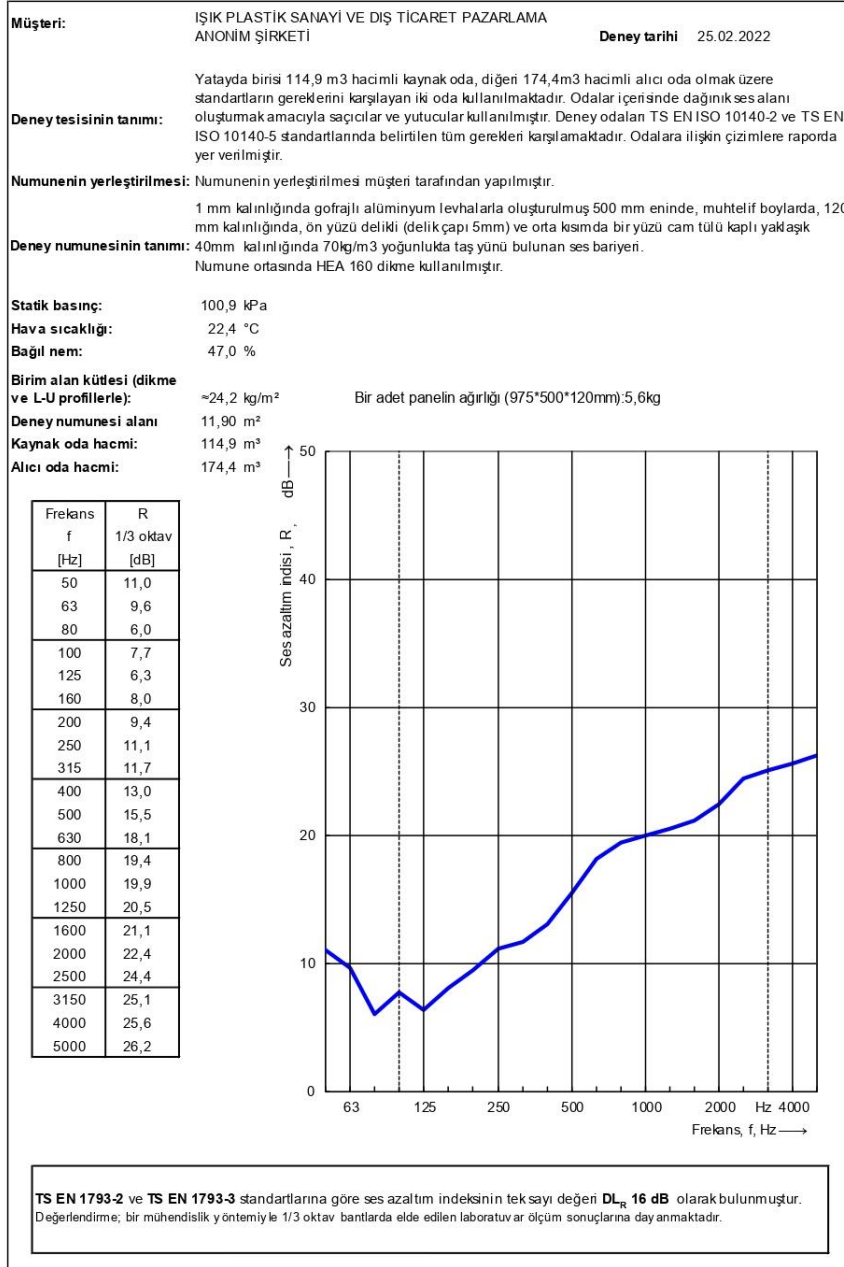
Figure B5: Experimental Test Report results



TSE DENEY ve KALİBRASYON MERKEZİ BŞKANLIĞI YAPI MALZ. YANGIN VE AKUSTİK LAB.
HEADSHIP OF TSE TEST and CALIBRATION CENTER CONST. MAT. FIRE AND ACOUSTICS LABORATORY

MUAYENE - DENEY SONUÇLARI TEST RESULTS
TS EN 1793-2:2018 ; TS EN 1793-3:2002

AB-0001-T
9437
03-22



6/11

LAB-D-FR-36 / 11.06.2020 - 6

Figure B6: Experimental Test Report results graph



TSE DENEY ve KALİBRASYON MERKEZİ BŞKANLIĞI YAPI MALZ. YANGIN VE AKUSTİK LAB.
HEADSHIP OF TSE TEST and CALIBRATION CENTER CONST. MAT. FIRE AND ACOUSTICS LABORATORY

MUAYENE - DENEY SONUÇLARI TEST RESULTS
TS EN 1793-2:2018 ; TS EN 1793-3:2002

| |
|-----------|
| AB-0001-T |
| 9437 |
| 03-22 |

R'_{max} Karşılaştırma Tablosu

| Frequency [Hz] | R [dB] | R' _{max} [dB] | R'>R [dB] |
|-------------------|-----------|---------------------------|--------------|
| 50 | 11,0 | 43,8 | 32,8 |
| 63 | 9,6 | 40,6 | 31,0 |
| 80 | 6,0 | 46,1 | 40,1 |
| 100 | 7,7 | 50,8 | 43,1 |
| 125 | 6,3 | 49,5 | 43,2 |
| 160 | 8,0 | 51,1 | 43,1 |
| 200 | 9,4 | 53,5 | 44,1 |
| 250 | 11,1 | 53,6 | 42,5 |
| 315 | 11,7 | 58,9 | 47,2 |
| 400 | 13,0 | 62,8 | 49,8 |
| 500 | 15,5 | 64,9 | 49,4 |
| 630 | 18,1 | 69,1 | 51,0 |
| 800 | 19,4 | 73,1 | 53,7 |
| 1000 | 19,9 | 77,2 | 57,3 |
| 1250 | 20,5 | 80,4 | 59,9 |
| 1600 | 21,1 | 83,6 | 62,5 |
| 2000 | 22,4 | 88,2 | 65,8 |
| 2500 | 24,4 | 90,2 | 65,8 |
| 3150 | 25,1 | 91,2 | 66,1 |
| 4000 | 25,6 | 89,8 | 64,2 |
| 5000 | 26,2 | 89,4 | 63,2 |

Lejant:

R: ses azaltım indisı

R'>R: maksimum ses azaltım indisı

7/11

LAB-D-FR-36 / 11.06.2020 - 6

Figure B7: Experimental Test Report results table

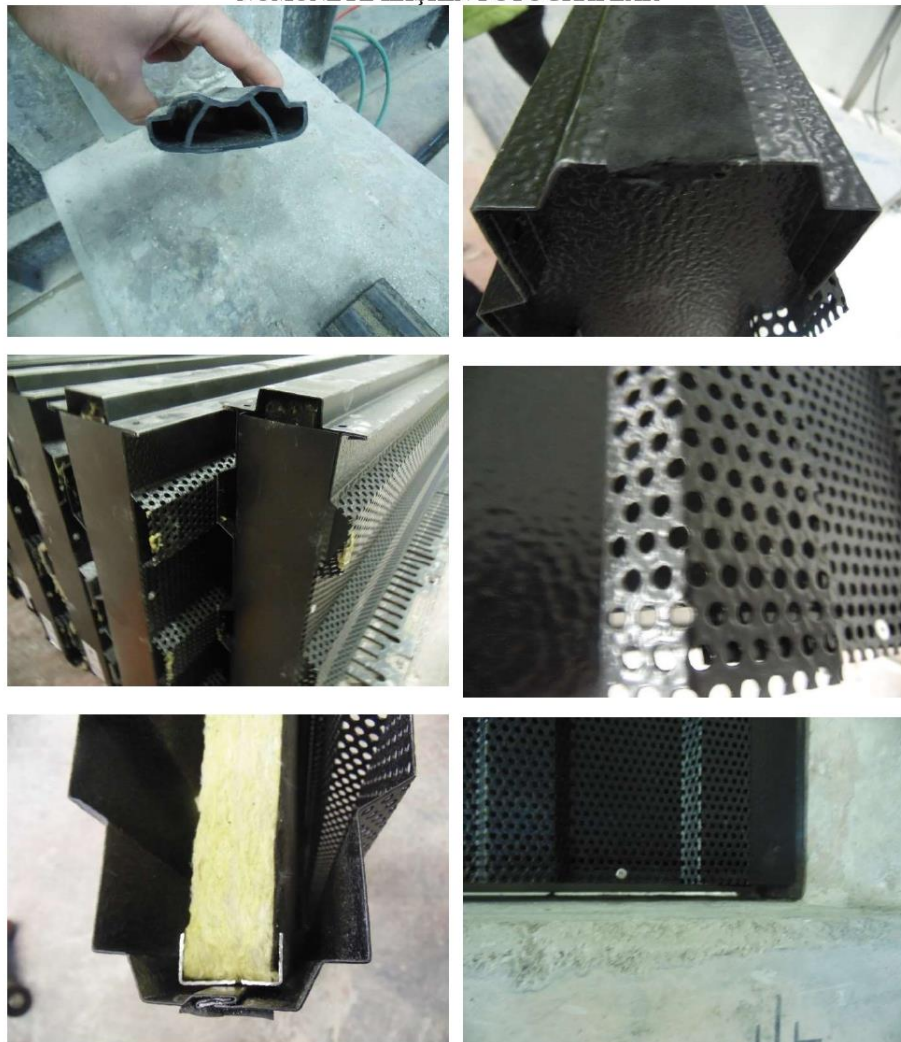


TSE DENEY ve KALİBRASYON MERKEZİ BŞKNLĞI YAPI MALZ. YANGIN VE AKUSTİK LAB.
HEADSHIP OF TSE TEST and CALIBRATION CENTER CONST. MAT. FIRE AND ACOUSTICS LABORATORY

MUAYENE - DENEY SONUÇLARI TEST RESULTS
TS EN 1793-2:2018 ; TS EN 1793-3:2002

AB-0001-T
9437
03-22

NUMUNEYE İLİŞKİN FOTOĞRAFLAR



8/11

LAB-D-FR-36 / 11.06.2020 - 6

Figure B8: Experimental Test Report photos



TSE DENEY ve KALİBRASYON MERKEZİ BŞKNLĞI YAPI MALZ. YANGIN VE AKUSTİK LAB.
HEADSHIP OF TSE TEST and CALIBRATION CENTER CONST. MAT. FIRE AND ACOUSTICS LABORATORY

MUAYENE - DENEY SONUÇLARI TEST RESULTS
TS EN 1793-2:2018 ; TS EN 1793-3:2002

AB-0001-T
9437
03-22

NUMUNEYE İLİŞKİN FOTOĞRAFLAR



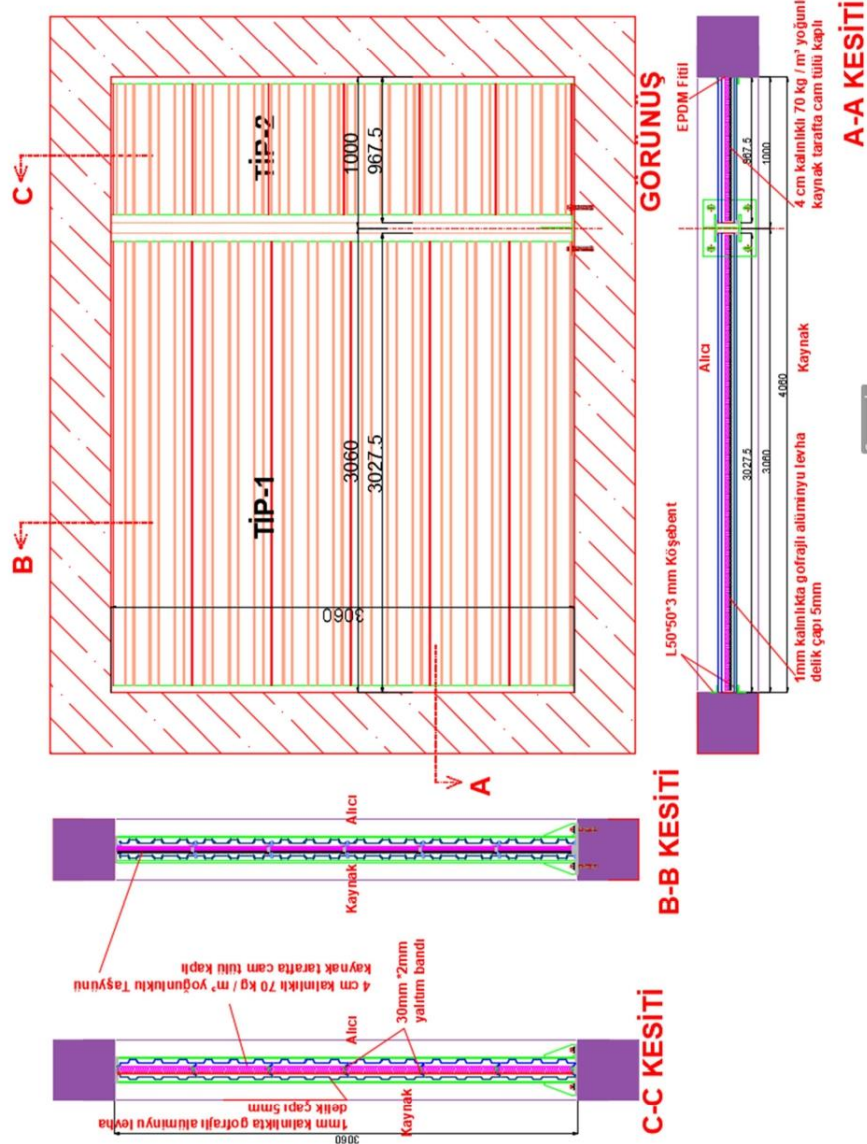
9/11

LAB-D-FR-36 / 11.06.2020 - 6

Figure B9: Experimental Test Report photos



NUMUNE GÖRÜNÜŞ VE KESİTİ



10/11

LAB-D-FR-36 / 11.06.2020 - 6

Figure B10: Experimental Test Report sample drawings



DENEY ODALARI PLAN VE KESİTİ

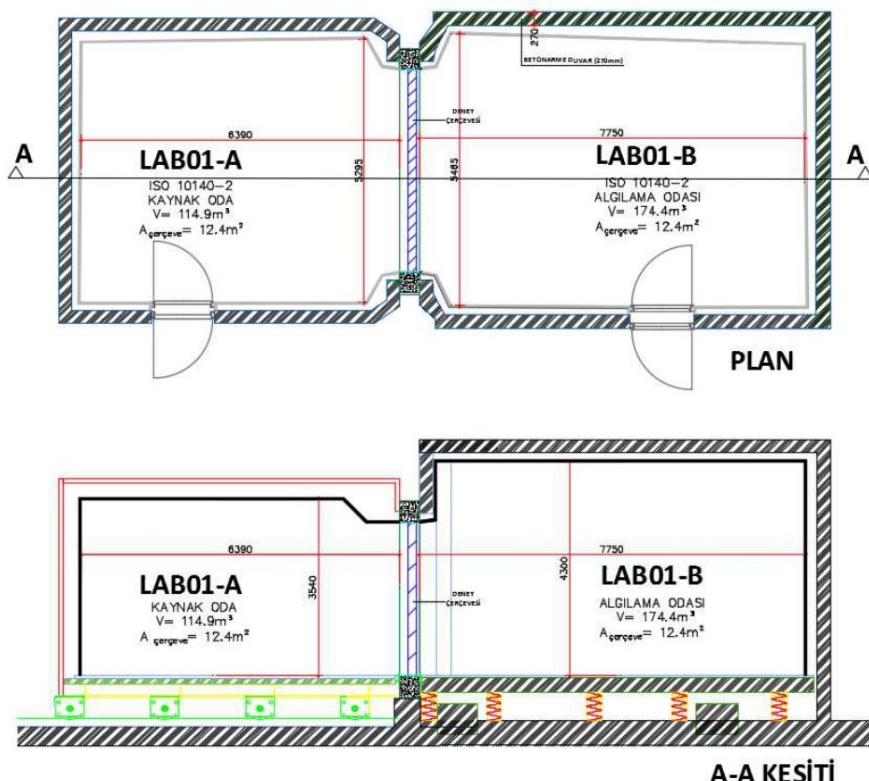


Figure B11: Experimental Test Report results room drawings